3 1176 00149 6901

UNCLASSIFIED
~~CONFIDENTIAL~~

Reference
23

NASA TECHNICAL MEMORANDUM

NASA TM X-1186

NASA TM X-1186

CLASSIFICATION CHANGED
UNCLASSIFIED
To
By authority of NASA Hdqtrs Date 10-21-69
s/Jack E. Smart
7-14-70

CHARGE RECOMBINATION ON WATER DROPLETS IN A PLASMA

by John S. Evans
Langley Research Center
Langley Station, Hampton, Va.

LIBRARY COPY
DEC 29 1965
LANGLEY RESEARCH CENTER
LIBRARY, NASA
LANGLEY STATION
HAMPTON, VIRGINIA

NATIONAL AERONAUTICS AND SPACE ADMINISTRATION • WASHINGTON, D. C. • DECEMBER 1965

UNCLASSIFIED ~~CONFIDENTIAL~~

UNCLASSIFIED

~~CONFIDENTIAL~~

NASA TM X-1186

CLASSIFICATION CHANGED
UNCLASSIFIED

To _____

By authority of NASA Hdqtrs Ltr Date 10-21-69
s/Jacob E. Smart RLP 7-14-70

CHARGE RECOMBINATION ON WATER DROPLETS IN A PLASMA

By John S. Evans

Langley Research Center
Langley Station, Hampton, Va.

GROUP 4
Downgraded at 3 year intervals;
declassified after 12 years

CLASSIFIED DOCUMENT–TITLE UNCLASSIFIED
This material contains information affecting the national defense of the United States within the meaning of the espionage laws, Title 18, U.S.C., Secs. 793 and 794, the transmission or revelation of which in any manner to an unauthorized person is prohibited by law.

NOTICE
This document should not be returned after it has satisfied your requirements. It may be disposed of in accordance with your local security regulations or the appropriate provisions of the Industrial Security Manual for Safe-Guarding Classified Information.

NATIONAL AERONAUTICS AND SPACE ADMINISTRATION

UNCLASSIFIED

~~CONFIDENTIAL~~

UNCLASSIFIED

CHARGE RECOMBINATION ON WATER DROPLETS IN A PLASMA*

By John S. Evans
Langley Research Center

SUMMARY

A simple model is proposed to explain the relief of radio blackout observed upon injecting water into the plasma layer surrounding the RAM B2 vehicle during flight. The basis of the model is recombination of ions and electrons on the surfaces of water droplets. At altitudes typical of maximum blackout, the principal parameters which control the effectiveness of the water-injection technique for signal recovery are found to be drop size, ratio of mass flow of water to mass flow of gas in the water-gas mixture, and flow time of drops from injection point to antenna. Fine sprays are shown to be more effective than coarse sprays, and electron concentration decreases approximately exponentially with distance from the injection point. The theory predicts that VHF signal recovery during injection from side nozzles on the RAM B2 flight should have required smaller injection rates as altitude increased. This conclusion is borne out by the observed rates. The drop radius required to correlate the theoretical and experimental results, on the basis of an assumed uniform drop size, is in the range of 10^{-6} to 10^{-5} meters.

INTRODUCTION

The RAM B2 (Radio Attenuation Measurement) flight experiment (ref. 1) has demonstrated that relief of radio blackout during reentry can be achieved by injecting water into the ionized air flow. Similar effects have been demonstrated in the laboratory (refs. 2 and 3), and it has been shown that materials other than water may be used. For example, experimental results on Freon were reported in reference 2, and a theoretical evaluation of carbon tetrachloride was reported in reference 4.

In the flight experiment, VHF signal attenuation was reduced when water was injected either from the stagnation point of a spherically blunted slender cone or from the surface of the cone. Stagnation-point injection is not discussed in this paper, except that it is noted that the experiment showed stagnation-point injection to be more effective than side injection on the RAM B2 flight. On a small-nosed vehicle like RAM B2, stagnation-point injection probably interferes with the electron-forming processes, either by cooling the equilibrium plasma in the nose region or by changing the shape of the shock

*Title, Unclassified.

UNCLASSIFIED

wave in front of the nose from a rounded to a pointed configuration like the shock wave produced by a pointed cone.

For side injection, at the speeds and altitudes corresponding to VHF blackout, the plasma over the RAM B2 vehicle was a nonequilibrium plasma in which electron concentration was larger than the local equilibrium value. Additional cooling of such a nonequilibrium plasma does not reduce electron concentration. Instead, one must look for ways in which the presence of water in the plasma could either enhance recombination of electrons with ions or cause attachment of electrons to molecules or atoms present in the flow. Since no attachment of electrons to molecules or recombination process involving molecules or atoms was found which appeared to be capable of producing the observed large reductions in electron concentration, attention was turned to the possibility that the effect might be produced by the presence of water in the form of droplets.

Most previous treatments of the effect of material particles on gas-phase ionization have been limited to consideration of plasmas in thermodynamic equilibrium. (See refs. 5 to 11.) Under this condition, the concentration of free electrons is determined by detailed balancing; thus, the effect on electron concentration of adding material particles to an equilibrium plasma is to shift to a new equilibrium concentration, which may be either greater or less than the original one.

A few papers (refs. 12 to 15) have considered the effects of adding solid particles to nonequilibrium plasma. The present treatment of water droplets in nonequilibrium plasma has much in common with these papers, but the theory has been developed along somewhat different lines because of the intended application and because of certain differences in behavior of liquid drops and solid particles. For example, thermionic emission has been neglected, even though it is very important in the treatment of solid particles in plasmas. The effect of a difference in flow speed between particles and plasma is accounted for in the present theory but was not included in references 12 to 15.

The present paper gives a theoretical analysis of the drop-charging process and of the recombination of electrons and ions on drops. The mean free path of electrons and ions is assumed to be large compared with the dimensions of the particles. The results of the analysis are compared with the results obtained from the RAM B2 flight experiment in order to determine whether the proposed mechanism of recombination on water drops can explain the observed effects.

SYMBOLS

The analysis presented herein is given in the International System of Units (SI). When the theory is applied to the RAM B2 flight, the results are given in both SI and U.S. Customary Units.

A cross-sectional area of stream tube, m^2

a speed parameter, $\frac{m}{2kT}$ where $m = m_e$ or m_i, sec^2m^{-2}

B_e speed parameter, $\left(\frac{n\sigma}{a_e'}\right)^{1/2}$, dimensionless

b_e speed parameter, $\left(u_e'\right)^2 + \left(u_g'\right)^2$, $m^2 sec^{-2}$

c concentration (number per unit volume), m^{-3}

d_e speed parameter, $2u_e'u_g'$, $m^2 sec^{-2}$

e magnitude of electron charge, 1.6×10^{-19} coulomb

erf(x) error function, $\frac{2}{\sqrt{\pi}} \int_0^x \exp\left(-y^2\right)dy$, dimensionless

F cross-section parameter (see appendix A), dimensionless

f transmission frequency, Hz

g_e normalized speed distribution function, dimensionless

J_e normalization constant for g_e, $\left(\frac{m_e}{2\pi kT}\right)^{3/2}$, $sec^3 m^{-3}$

K cross-section parameter, dimensionless

k Boltzmann's constant, 1.38×10^{-23} joule deg^{-1}

L cross-section parameter, dimensionless

M rate of water injection, kg sec^{-1}

M^* ratio of mass flow of water to mass flow of gas with which it mixes, dimensionless

m_e mass of electron, 9.1×10^{-31} kg

m_i mass of typical ion, 5.0×10^{-26} kg

n number of electron charges on drop, dimensionless

n^* total number of electrons drop has removed from plasma, dimensionless

p pressure, N/m^2

Q collision cross section, m^2

R	minimum drop radius for mechanical stability, m
r	drop radius, m
T	temperature, ^{o}K
t	time, sec
U	speed ratio, $\frac{u_g'}{\bar{u}}$, where $\bar{u} = \bar{u}_e$ or $\bar{u}_i$, dimensionless
u	speed, m sec^{-1}
$\bar{u}_e$	mean thermal speed of electrons, $\left(\frac{8kT}{\pi m_e}\right)^{1/2}$, m sec^{-1}
$\bar{u}_i$	mean thermal speed of ions, $\left(\frac{8kT}{\pi m_i}\right)^{1/2}$, m sec^{-1}
V_p	potential of drop surface relative to plasma, volt
v	speed ratio, $\frac{u'}{u_g'}$, dimensionless
W	work, joule
X,Y,Z	Cartesian coordinates
x,y,z	distances along X, Y, and Z axes
α	drop acceleration, m sec^{-2}
β	factor by which c_e changes between x_3 and x_4, dimensionless
Δ	exponential decay constant, m
δ	distance from injection point to antenna, m
δ^*	exponential decay distance, $\delta - x_4$, m
γ	surface tension of water, newton m^{-1}
ϵ_o	permittivity of free space, 8.8×10^{-12} farad m^{-1}
θ	angle coordinate, radian
Λ	mass-flow parameter, $c_p u_p'' A$, sec^{-1}
λ	mean free path, m

λ_D Debye length, $69\left(\frac{T}{c_e}\right)^{1/2}$, m

μ mass ratio, $\left(\frac{m_i}{m_e}\right)^{1/2}$, dimensionless

ϕ angle coordinate, radian

ρ density, kg m^{-3}

ρ_W density of water, 1×10^3 kg m^{-3}

σ charge parameter, $\frac{e^2}{4\pi\epsilon_o rkT}$, dimensionless

τ relaxation time, sec

τ^* denotes either τ_e or τ_i when $\tau_e \approx \tau_i$, sec

Subscripts:

c denotes critical electron concentration for plasma resonance

d denotes cross section for contact collision between drop and ion or electron

e electron

i ion

g gas

m denotes maximum value of n for mechanically stable drop

p particle (in this paper, particles are water droplets)

s denotes value at surface of vehicle

t denotes total annular cross-sectional area of gas flow in shock layer

0 n = 0

1 n = peak value

2 n = peak value $\left(\text{for } n_1 c_p \ll c_{e0}\right)$

3 denotes value at point water is injected into flow

4 denotes value at point where drop speed becomes equal to gas speed

5 denotes value at point where radio transmission is desired

A dot over a symbol (for example, $\dot{c}$) signifies differentiation with respect to time. A prime on a symbol (for example, u') signifies that it is measured in a coordinate system in which the drops are at rest. Double primed quantities are referred to a system at rest relative to the vehicle surface. Unprimed symbols are referred to a system in which the plasma is at rest. (See appendix A.) A bar over a symbol (for example, $\bar{u}$) or a group of symbols signifies that it has been averaged over the appropriate distribution of speeds.

THEORY

Assumptions

The hypothesis is advanced that water droplets, when present in an ionized gas, can act as centers for charge recombination. The following conditions are chosen as the basis for discussion of the hypothesis:

(1) The drops are all the same size and are deposited uniformly in the flow at the injection site with zero initial speed

(2) The drop size does not change with time

(3) The plasma density and temperature are not changed by water injection

(4) The drops accelerate uniformly until they move at the same speed as the gas

(5) The two-phase flow of drops and gas is treated as a one-dimensional flow

(6) Thermionic and secondary emission of electrons from the drops is absent

(7) All ions have the charge $+e$

(8) Every electron which reaches the surface of a drop is absorbed

(9) Every ion which reaches the surface of a drop is neutralized

(10) All the gas particles, including the electrons, have Maxwellian velocity distributions corresponding to the translational temperature of the gas

(11) The mean free paths of electrons and ions in the gas are large compared with the diameter of the drops

(12) The effective cross section of the drops for recombination is a linear function of drop speed.

Development of Rate Equations

The following sketch is useful for considering what happens to a drop at rest as it is bombarded by electrons and ions. If the drop has no charge it will be struck more often by electrons than by ions because electrons have higher mobility than ions. Consequently, a net charge $-ne$ will accumulate on the drop, where n is a positive integer and $-e$ is the electronic charge. The asymptotic value of n is determined by dynamic balance between the capture rates for electrons and ions. The capture cross section for electrons decreases with n and the capture cross section for ions increases with n until the two capture rates are equal.

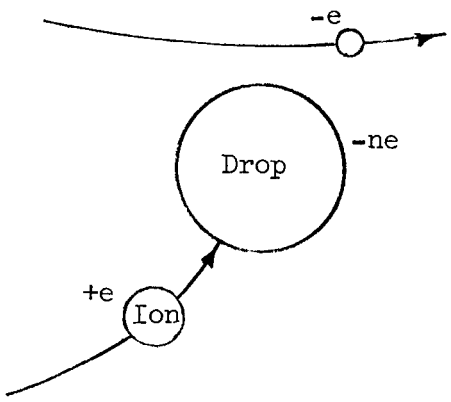

Sketch (a)

For a plasma at constant density, these ideas are expressed in mathematical form as follows:

$$\frac{dc_e}{dt} = -\left(\overline{u'Q_d}\right)_e c_p c_e \tag{1}$$

$$\frac{dc_i}{dt} = -\left(\overline{u'Q_d}\right)_i c_p c_i \tag{2}$$

where $\overline{u'Q_d}$ is the velocity-averaged specific rate for contact collisions of electrons or ions with water droplets. These contact collision specific rates are evaluated in appendix A and are

$$\left(\overline{u'Q_d}\right)_e = \pi r^2 \bar{u}_e \exp(-n\sigma) = \pi r^2 \bar{u}_e F_e$$

$$\left(\overline{u'Q_d}\right)_i = \pi r^2 \bar{u}_i \left(K_i + L_i n\sigma\right) = \pi r^2 \bar{u}_i F_i$$

where F_e and F_i are functions of $U_e = \frac{u_g'}{u_e}$ and $U_i = \frac{u_g'}{u_i}$, respectively. The F factors are plotted against U_e and U_i in figure 1.

It is worthwhile to note that $n\sigma$ can be expressed as $-\frac{eV_p}{kT}$, where V_p is the potential of the drop surface relative to the plasma. The value that

V_p takes is determined by the balance achieved between electron and ion collection rates.

When the expressions for $\overline{u'Q_d}$ are substituted into equations (1) and (2), the results are

$$\frac{dc_e}{dt} = -\pi r^2 \bar{u}_e c_p c_e \exp(-n\sigma) \tag{3}$$

$$\frac{dc_i}{dt} = -\pi r^2 \bar{u}_i c_p c_i (K_i + L_i n\sigma) \tag{4}$$

(As indicated in appendix A, the value of L_i in equation (4) must be set equal to zero if $\lambda_D \ll r$.)

The drop-charging process is analyzed in appendix B. There it is shown that the charge on a drop rises quickly upon entry into a plasma to a value $-n_1 e$, as given by solution of the equation

$$\left(1 - \frac{n_1 c_p}{c_i}\right)\mu \exp(-n_1\sigma) = K_i + L_i n_1 \sigma \tag{5}$$

When $n_1 c_p \ll c_{e0}$, equation (5) becomes

$$\mu \exp(-n_2\sigma) = K_i + L_i n_2 \sigma \tag{6}$$

where n_2 is used to designate the value of n_1 for this condition.

The differential equations used for analysis of the charging process also reveal the nature of the subsequent decay of electron concentration. The form of these equations which apply to the RAM B2 experiment is designated as case I in appendix B. For case I, equations (3) and (4) can be written as

$$\tau^* \dot{c}_e + c_e = 0 \tag{7}$$

$$\tau^* \dot{c}_i + c_i = 0 \tag{8}$$

where τ^* is the characteristic decay time for the decrease in electron and ion concentrations.

The value of τ^* is given by the equations

$$\left.\begin{aligned} \tau^* &= \left[\mu \pi r^2 c_p \bar{u}_i \exp(-n_2\sigma)\right]^{-1} \\ \tau^* &= \left[\pi r^2 c_p \bar{u}_i (K_i + L_i n_2 \sigma)\right]^{-1} \end{aligned}\right\} \tag{9}$$

DERIVATION OF WORKING EQUATIONS

The decrease of c_e along a stream tube in the flow is given by the solution of equation (7) where the relaxation time τ^* has the value given by equation (9). For constant τ^*, equation (7) has the solution

$$c_e = c_{e0} \exp \frac{-t}{\tau^*}$$

The relaxation time is not constant, however, until u_g' approaches zero because of the dependence of $K_i + L_i n\sigma$ on u_g' and the variation of c_p with u_p''.

Consider the charge-conservation equation in a one-dimensional stream tube

$$u_g'' c_e A + \Lambda n^* = \text{Constant}$$

where $\Lambda = c_p u_p'' A = \text{Constant}$, and n^* is defined as the total number of electrons which a drop has removed from the plasma during its residence there. (This charge-conservation equation is invalid for $u_p'' = 0$ and must be generalized if drops with $u_p'' < 0$ are present.)

In the steady state, the relationship between the spatial derivatives of the terms in the preceding equation is

$$\frac{d}{dx}\left(u_g'' c_e A\right) = -\Lambda \frac{dn^*}{dx}$$

The time rate of change of $u_g'' c_e A$ along a drop path is

$$\frac{d}{dt}\left(u_g'' c_e A\right) = u_p'' \frac{d}{dx}\left(u_g'' c_e A\right) = -\Lambda \frac{dn^*}{dt}$$

Equation (7) can be used to evaluate $\frac{dn^*}{dt} = -\frac{\dot{c}_e}{c_p}$, thus,

$$\frac{d\left(u_g'' c_e A\right)}{u_g'' c_e A} = -\Lambda \pi r^2 \bar{u}_i F_i \frac{dx}{u_g'' u_p'' A}$$

which has the solution at a general point $x \geq x_3 = 0$

$$c_e = c_{e3} \frac{u_{g3}'' A_3}{u_g'' A} \exp\left(-\pi\Lambda \int_0^x \frac{r^2 \bar{u}_e F_i \, dx}{u_g'' u_p'' A}\right) \tag{10}$$

If the gas dynamics and thermodynamics of the injection and mixing process can be specified, this equation can be solved by numerical integration on an electronic data processing machine. When this is done, it is advantageous to remove some of the restrictions placed on the problem in this paper. For example, the effect of evaporation on drop size can be included. However, in order to gain insight into the nature of the problem, equation (10) has been solved by approximate analytical methods. The approximate treatment of the gas dynamics and thermodynamics is given in appendix C.

In order to evaluate the integral in equation (10), the following linear expression is used for F_i:

$$F_i = F_{i3} - \left(F_{i3} - F_{i4}\right)\frac{u_p''}{u_{p4}''}$$

where F_{i3} is the value of F_i at the injection point and F_{i4} is the value of F_i when $u_p'' = u_{p4}''$. From figure 1, it can be seen that if $\lambda_D \ll r$ (that is, $L_i = 0$), $F_{i3} = K_{i3}$ and $F_{i4} = 1$. If $\lambda_D \gg r$, $F_{i3} = \left(K_i + L_i n\sigma\right)_3$ and $F_{i4} = 4.87$ (for $\mu = 235$).

Substituting the linear approximation for F_i into equation (10) and noting that constant density implies that $u_g''A = u_{g3}''A_3$ yields

$$\frac{c_e}{c_{e3}} = \exp\left\{-\left(\frac{\Lambda\pi r^2\bar{u}_i}{u_{p4}''u_{g3}''A_3}\right)\left[F_{i3}u_{p4}''t - \left(F_{i3} - F_{i4}\right)x\right]\right\} \tag{11}$$

In order to use equation (11), it is necessary to establish a relationship between x and t (where t is the time required for a drop to move from the injection point to the point x) by assuming (see appendix C) that the drops undergo constant acceleration from rest between x_3 (the injection point) and x_4 (the point at which drop and gas speeds are equal). Over the remaining distance to the point x_5, where an antenna might be located, the drop and gas speeds are both equal to the constant value u_{p4}''. The acceleration, velocity, and distance relations corresponding to the constant-acceleration assumption are

$$\alpha_3 = \frac{3\rho_{g3}\left(u_{g3}''\right)^2}{4r\rho_W}$$

$$u_p'' = \alpha_3 t = \sqrt{2\alpha_3 x} \qquad \left(0 \leqq x \leqq x_4\right)$$

$$x = \frac{1}{2}u_p''t = \frac{1}{2}\alpha_3 t^2 \qquad \left(0 \leqq x \leqq x_4\right)$$

The reduction in electron concentration achieved at x_5 can be expressed as

$$\frac{c_{e5}}{c_{e3}} = \beta \exp\left(\frac{-\delta^*}{\Delta}\right) \qquad (\delta^* \geqq 0) \qquad (12)$$

where

$$\left.\begin{aligned} \beta &= \exp\left[-\frac{\bar{u}_i\left(F_{i3} + F_{i4}\right)}{2u''_{g3}} \frac{M^*}{1 + M^*}\right] \\ \Delta &= \frac{4\rho_W u''_{g3}}{3\rho_{g3}\bar{u}_i F_{i4}} \frac{r}{M^*(1 + M^*)} \\ \delta^* &= x_5 - x_4 \end{aligned}\right\} \qquad (13)$$

The parameters β and Δ are plotted as functions of r and M^* in figures 2 to 4. Since there is a secondary dependence on plasma properties, plots are given for two points on the RAM B2 flight trajectory. It should be noted that equation (12) does not hold for $\delta^* < 0$, which corresponds to the downstream point of interest being so close to the injection point that $x_5 < x_4$. The region where $\delta^* < 0$ for the RAM B2 flight is indicated in the figures.

A reasonable criterion to ensure that radio signals will be transmitted without attenuation through the plasma at the downstream point of interest is obtained by requiring that $c_{e5} = c_{ec}$, the critical frequency for plasma resonance at the transmission frequency f and is expressed by

$$c_{e5} = c_{ec} = \frac{f^2}{80.53}$$

From equation (13), the value of Δ required to reduce c_e to c_{ec} at the RAM B2 VHF slot antenna is

$$\Delta_c(r,M^*) = \frac{\delta^*}{-\log_e \dfrac{f^2}{80.53 c_{e3}\beta}} \qquad (\delta^* \geqq 0) \qquad (14)$$

The values of Δ_c obtained from equation (14) are shown in figures 3 and 4.

The reduction of electron concentration as a function of distance is shown in figures 5 and 6. Both figure 2 and figures 5 and 6 show that a "law of

diminishing returns" applies as increasing amounts of water are injected into the flow.

Figure 7 shows the values of M^* required to achieve values of c_e/c_{e3} in the range $10^{-3} \leqq \frac{c_e}{c_{e3}} \leqq 1$ at two altitudes. These curves were obtained by solving equation (12) as an equation in M^*. If the drops are fully accelerated before reaching the antenna,

$$\frac{F_{i3}M^*}{2(1 + M^*)} + \frac{3x_5\rho_{g3}F_{i4}}{4r\rho_W} M^*(1 + M^*) = \frac{-u_{g3}}{\bar{u}_i} \log_e\left(\frac{c_{e5}}{c_{e3}}\right) \qquad (x_4 < x_5)$$

If the drops are not fully accelerated before reaching the antenna,

$$\frac{F_{i4} - F_{i3}}{2} \frac{3x_5\rho_{g3}}{2r\rho_W} M^*(1 + M^*) + F_{i3}M^*\left(\frac{3x_5\rho_{g3}}{2r\rho_W}\right)^{1/2} = \frac{-u_{g3}}{\bar{u}_i} \log_e\left(\frac{c_{e5}}{c_{e3}}\right) \quad (x_4 > x_5)$$

The meaning of the subscript s on the experimental range of M^* in figure 7 is explained in the next section.

APPLICATION OF ANALYSIS TO RAM B2 FLIGHT DATA

The flight measurements most suitable for comparison with results calculated from the preceding theory are those associated with recovery of the signal transmitted from a slot antenna located on the conical portion of the vehicle. The leading edge of this antenna was about 0.5 meter directly downstream from one of the two side-injection areas. These side-injection areas were on opposite sides of the vehicle, were about 0.13 meter from the nose, and each area contained 98 orifices for injecting liquid water in the direction perpendicular to the gas flow. The water was injected in short bursts during the data-taking period and the injection rate was varied in discrete steps by activating various combinations of the nozzles. More details about the experiment and the results obtained can be found in reference 1.

Figure 8 shows the calculated variation of M_s^* with altitude during the flight, where

$$M_s^* = \frac{M}{\left(\rho_{g3}u''_{g3}\right)_s A_{t3}}$$

The factor M is the mass of water injected per unit time from both side-injection areas. The factor A_{t3} is the annular cross-sectional area of the shock layer at the injection site. It is assumed that the water drops from

one side were distributed uniformly over one-half of the area A_{t3} and that the other half of the area A_{t3} was filled by injection from the other side. The subscript s on M^* and $\rho_{g3}u''_{g3}$ indicates that these quantities have values calculated for a streamline lying near the vehicle surface. Calculation of the charge recombination along these streamlines should be appropriate for comparison with signal recovery data because the largest values of electron concentration in the shock layer are found close to the surface.

The vehicle speed at both of the trajectory points used was 5340 m sec^{-1} (17,500 ft sec^{-1}); the two altitudes were 4.78×10^4 m (157,000 ft) and 6.40×10^4 m (210,000 ft). Table I lists the parameters needed for the comparisons:

TABLE I

PARAMETERS FOR CALCULATING CHARGE RECOMBINATION EFFECT OF

WATER INJECTION DURING RAM B2 FLIGHT

General parameters:		
ρ_W, kg m^{-3} (lb ft^{-3})	1000	(62.5)
μ	235	
δ, m (ft)	0.5	(1.64)
f, Hz or cps	2.44×10^8	
A_{t3}, m^2 (ft^2)	0.0214	(0.2303)
Parameters for an altitude of 4.78×10^4 m (157,000 ft):		
$(\rho_{g3})_s$, kg-m^{-3} (slug-ft^3)	3.10×10^{-6}	(1×10^{-4})
$(u''_{g3})_s$, m sec^{-1} (ft sec^{-1})	3040	(9974)
T_3, ^oK	2600	
$c_{e0} = c_{e3}$, m^{-3} (ft^{-3})	8×10^{17}	(2.27×10^{16})
Parameters for an altitude of 6.40×10^4 m (210,000 ft):		
$(\rho_{g3})_s$, kg m^{-3} (slug-ft^3)	4.66×10^{-7}	(1.5×10^{-5})
$(u''_{g3})_s$, m sec^{-1} (ft sec^{-1})	3300	(10,827)
T_3, ^oK	3000	
$c_{e0} = c_{e3}$, m^{-3} (ft^{-3})	8×10^{17}	(2.27×10^{16})

Figure 8 shows that at an altitude of 4.78×10^4 m (157,000 ft), M_s^* ranged from 0.8 for the smallest injection rate to 4.9 for the largest injection rate.

At an altitude of 6.40×10^4 m (210,000 ft), the range of M_s^* was from 3.6 to 22.3. Figure 8 also shows the approximate values of M_s^* for which complete signal recovery was achieved.

Reduction of c_e to c_{ec} is a reasonable criterion for reducing to negligible magnitude the direct attenuation of propagated radio waves by a plasma. For the RAM B2 VHF antenna, this criterion means that c_e/c_{e3} should be reduced to 10^{-3} in the distance $x_5 = 0.5$ meter. Examination of the records received at Coquina Beach from this antenna reveal that for side injection the signal showed some recovery at the smallest injection rates used and appeared to achieve complete recovery at about the third or fourth level out of the seven levels used in each pulse. (See fig. 9.) Complete recovery is defined here as the point at which adding water at a faster rate had little or no effect on received signal strength. (For nose injection, even the smallest injection rates used gave complete recovery in the sense defined here.) The maximum and minimum injection rates for side injection and those corresponding to observed complete signal recovery are summarized in table II.

TABLE II

SIDE INJECTION RATES DURING FLIGHT OF RAM B2

Injection pulse	Altitude range		Injection rate					
			Level 1		Complete recovery		Level 7	
	km	ft	lb/sec	kg/sec	lb/sec	kg/sec	lb/sec	kg/sec
1	45.57 to 46.18	149,500 to 151,500	(*)	(*)	0.770	0.350	1.602	0.728
2	48.16 to 49.23	158,000 to 161,500	0.178	0.081	.682	.310	1.052	.478
3	51.51 to 52.73	169,000 to 173,000	.156	.071	.550	.250	.920	.418
4	55.11 to 56.33	180,800 to 184,800	.145	.066	.462	.210	.803	.365
5	58.52 to 59.68	192,000 to 195,800	.123	.056	.363	.165	.768	.349
6	61.69 to 62.64	202,400 to 205,500	.128	.058	.363	.165	.715	.325
7	64.37 to 65.23	211,200 to 214,000	.054	.119	.407	.185	.682	.310

*Injection began at level 3.

The experimental injection rates and the rates corresponding to complete signal recovery are plotted against altitude in figure 9, and curves showing the calculated rates to achieve complete recovery $\left(\frac{c_e}{c_{e3}} = 10^{-3}\right)$ are also included.

RESULTS AND DISCUSSION

The comparison of theoretical and experimental results has been presented in different ways in figures 7, 8, and 9. In examining these figures, it should be remembered that the size of the water droplets and their distribution in the flow field is not known. In the theory, the drops are assumed to be uniform in size and uniformly distributed over any cross section of the flow field perpendicular to the flow direction. However, the mass flow of air through different parts of these flow-field cross sections is not uniform, and the smallest mass flows of air are those near the body surface.

The true nature of the water breakup and mixing process is an important part of the problem and deserves careful study. Spray penetration experiments which were a part of the design studies made for the RAM project are reported in reference 16. Liquid-jet breakup and drop-size distribution are discussed in references 17 to 20.

As was mentioned earlier, more accurate solutions of equation (10) can be obtained by machine integration. Figures 10 and 11 present comparisons of the results calculated from the approximate analytical theory with machine-computed results. The machine program used was that described in reference 21, after modification to compute with frozen nonequilibrium gas compositions correponding to those present in flight instead of computing with equilibrium gas composition, as described in reference 21. The effects of heat transfer, evaporation, and variable drag coefficient are included in the program. One additional modification added for this work was the inclusion of F_i factors (see appendix A and fig. 1) based on local values of U_i and r/λ_D.

It can be seen from figure 10 that density and temperature are not constant, as they were assumed to be in the approximate solution. Fortunately, the electron recombination is insensitive to these parameters. The divergence of the curves representing distance traveled by a drop is a more serious matter, since equations (12) and (13) show that the calculated reduction of electron concentration varies exponentially with distance.

Figure 11 shows the variation of electron concentration plotted against both distance and time. It can be seen that the assumption of constant acceleration causes the approximate method to underestimate the amount of reduction which can be achieved in a given distance. When plotted against time the two methods give nearly the same results except at $M^* = 1$. The divergence of results here is due to reduction of drop surface area caused by evaporation. This result is borne out by figure 12, which shows that, at $\frac{x}{r} \approx 10^5$, machine-computed surface areas dropped to 50 percent of their initial values.

CONCLUSIONS

Three conclusions can be drawn from the comparison of theoretical and experimental results: (1) the observed signal recovery can be accounted for

using the theory; (2) the calculated result that, as altitude increased on the RAM B2 flight, smaller injection rates of water should have been required to achieve complete signal recovery is confirmed by the experiment; (3) the radii of the water drops in the flow, as deduced from the comparison between theoretical and experimental results, were of the order of 10^{-6} to 10^{-5} meter.

The observed amounts of water required to achieve complete recovery did not always agree with the second conclusion, since at altitudes greater than 6.10×10^4 m (200,000 ft), the points shown in figure 9 show a trend toward larger rather than smaller amounts of water required. A possible explanation for this trend is that the penetration of water spray into the shock layer may have been so great at high altitude that very little water was deposited in the streamlines near the surface where the electron concentration was highest.

From the theoretical results, it can be concluded that the principal flight parameters to be considered are the drop size r, the ratio of mass flow of water to mass flow of gas in the water-gas mixture M^*, and the flow time of drops from injection point to antenna t. From a more general point of view (see eqs. (3) and (4)), the principal parameters can be taken to be drop size r, drop concentration c_p, and time t.

The comparison of approximate and machine-computed results revealed that the two methods give essentially the same reduction of electron concentration for equal intervals of time after injection of drops into the flow, except that for long time intervals, evaporation reduces the effectiveness of the drops by reducing their surface area. The comparison of the two results on the basis of equal distances from the injection point is not so favorable, because of the assumption of constant drop acceleration used in the approximate method. This result serves as a reminder that the fundamental variable for the recombination process is time of exposure of the drops to the plasma, rather than the distance the drops have traveled. It also shows that the approximate method is a useful substitute for machine calculations, if careful attention is paid to establishing the proper relationship between time and distance.

Langley Research Center,
National Aeronautics and Space Administration,
Langley Station, Hampton, Va., August 25, 1965.

APPENDIX A

CALCULATION OF CONTACT COLLISION SPECIFIC RATES

A water droplet in a plasma is simply a small floating spherical probe. The theory of plasma probes is discussed in many published works. (For example, see ref. 22.) The electron current to a floating probe under free-molecule conditions is $\pi r^2 \bar{u}_e c_e \exp(-n\sigma)$. However, for a floating probe the value of $n\sigma = -\frac{eV_p}{kT}$ is determined by the magnitude of the ion current, because the net current to such a probe is zero.

It would be easy to average over the thermal speed distribution of the ions to obtain the ion current, except that it is necessary to account for the effect of the sheath on the probe and for the effect of relative motion between probe and plasma.

It is instructive to begin by neglecting the presence of the sheath and calculating the electron and ion currents collected by a moving drop. The following sketch is useful for visualizing the relationships between the various velocities involved. All the drops are assumed to have the same velocity; namely, they are at rest in the primed system. The mean velocity of the electrons and ions is the same as the mass motion of the gas. Relative to a drop, this velocity is $u_g' = u_g'' - u_p''$, where u_g'' and u_p'' are the gas and water droplet velocities, respectively, relative to the vehicle surface. In the unprimed system, the thermal velocities of the electrons (or ions) are uniformly distributed in direction but not in magnitude.

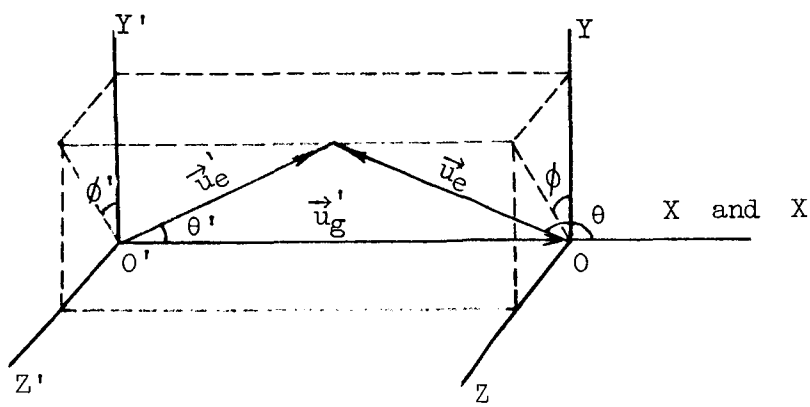

The probability that the end of the $\vec{u}_e$ vector falls in the element of volume $u_e^2 \sin\theta \, d\theta \, d\phi \, du_e$ is

$$g_e(u_e)u_e^2 \sin\theta \, d\theta \, d\phi \, du_e = J_e \exp\left(-a_e u_e^2\right) u_e^2 \sin\theta \, d\theta \, d\phi \, du_e$$

where $g_e(u_e)$ is the normalized Maxwellian distribution function which describes the density in velocity space of the points where $\vec{u}_e$ vectors terminate. The normalization constant J_e is defined by

$$J_e = \left(\frac{m_e}{2\pi kT}\right)^{3/2}$$

and the velocity parameter a_e is defined by

$$a_e = \frac{m_e}{2kT}$$

The velocity-averaged specific rate $\overline{u'Q_d}$ for electrons can be written as

$$\left(\overline{u'Q_d}\right)_e = \int u_e' Q_d(u_e') \, g_e(u_e', \theta') \, (u_e')^2 \sin\theta' \, d\theta' \, d\phi' \, du_e'$$

where $g_e(u_e', \theta')$ is the normalized non-Maxwellian distribution function for the density in velocity space of terminal points of $\vec{u}_e'$ vectors.

In the primed system, $g_e(u_e)$ becomes

$$g_e(u_e', \theta') = J_e \exp\left[-a_e\left(b_e - d_e \cos\theta'\right)\right]$$

where

$$b_e = (u_e')^2 + (u_g')^2$$

$$d_e = 2u_e' u_g'$$

For an electron moving in the electric field around a charged drop,

$$\left(u'Q_d\right)_e = \pi r^2 u_e' \left[1 - \frac{n\sigma}{a_e (u_e')^2}\right] \qquad \left((u_e')^2 \geqq \frac{n\sigma}{a_e}\right)$$

$$\left(u'Q_d\right)_e = 0 \qquad \left((u_e')^2 \leqq \frac{n\sigma}{a_e}\right)$$

Since $(u'Q_d)_e$ is independent of θ' and ϕ', the distribution function $g_e(u_e', \theta')$ can be integrated over θ' and ϕ' to give

$$g_e(u_e') = 2\pi J_e(u_e')^2 \exp(-a_e b_e) \int_0^{\pi} \left[\exp(a_e d_e \cos\theta')\right] \sin\theta' \, d\theta'$$

The normalized non-Maxwellian distribution function for u_e' is

$$g_e(u_e') = \left\{2\left(\frac{m_e}{2\pi kT}\right)^{1/2} \frac{\exp\left[-a_e(u_g')^2\right]}{u_g'}\right\} u_e' \exp\left[-a_e(u_e')^2\right] \sinh 2a_e u_g' u_e'$$

This equation can also be written as

$$g_e(v_e') = J_e' v_e' \exp\left[-a_e'(v_e')^2\right] \sinh 2a_e' v_e'$$

where

$$J_e' = \bar{u}_e\left[a_e u_g' \exp(-a_e')\right]$$

$$\bar{u}_e = \left(\frac{8kT}{\pi m_e}\right)^{1/2}$$

$$a_e' = a_e(u_g')^2$$

$$v_e' = \frac{u_e'}{u_g'}$$

The velocity-averaged value of $(u'Q_d)_e$ is

$$\left(\overline{u'Q_d}\right)_e = \pi r^2 \bar{u}_e \left[a_e' \exp(-a_e')\right] \int_{B_e}^{\infty} (v_e')^2 \exp\left[-a_e'(v_e')^2\right] \left[1 - \frac{n\sigma}{a_e'(v_e')^2}\right] \sinh 2a_e' v_e' \, dv_e'$$

where

$$B_e = \left(\frac{n\sigma}{a_e'}\right)^{1/2}$$

Evaluation of this integral yields

$$\left(\overline{u'Q_d}\right)_e = \left(\pi r^2 \bar{u}_e\right) F_e$$

where

$$F_e = \frac{1}{2}\exp(-n\sigma)\exp\left(-\frac{4U_e^2}{\pi}\right)\left[\frac{\sqrt{\pi n\sigma}}{2U_e}\sinh\left(4U_e\sqrt{\frac{n\sigma}{\pi}}\right) + \cosh\left(4U_e\sqrt{\frac{n\sigma}{\pi}}\right)\right]$$

$$+ \frac{\pi}{8U_e}\left(\frac{1}{2} - n\sigma + \frac{4U_e^2}{\pi}\right)\left\{\operatorname{erf}\left[(n\sigma)^{1/2} + \frac{2U_e}{\sqrt{\pi}}\right] - \operatorname{erf}\left[(n\sigma)^{1/2} - \frac{2U_e}{\sqrt{\pi}}\right]\right\}$$

if

$$(n\sigma)^{1/2} > \frac{2U_e}{\sqrt{\pi}}$$

or

$$F_e = \frac{1}{2}\left[\exp(-n\sigma)\exp\left(-\frac{4U_e^2}{\pi}\right)\right]\left[\frac{\sqrt{\pi n\sigma}}{2U_e}\sinh\left(4U_e\sqrt{\frac{n\sigma}{\pi}}\right) + \cosh\left(4U_e\sqrt{\frac{n\sigma}{\pi}}\right)\right]$$

$$+ \frac{\pi}{8U_e}\left(\frac{1}{2} - n\sigma + \frac{4U_e^2}{\pi}\right)\left\{\operatorname{erf}\left[\frac{2U_e}{\sqrt{\pi}} + (n\sigma)^{1/2}\right] + \operatorname{erf}\left[\frac{2U_e}{\sqrt{\pi}} - (n\sigma)^{1/2}\right]\right\}$$

if

$$\frac{2U_e}{\sqrt{\pi}} > (n\sigma)^{1/2}$$

The velocity-averaged value of $(u'Q_d)_i$ is

$$\left(\overline{u'Q_d}\right)_i = \left(\pi r^2\bar{u}_i\right)\left[a_i' \exp\left(-a_i'\right)\right]\int_0^\infty \left(v_i'\right)^2 \exp\left[-a_i'\left(v_i'\right)^2\right]\left[1 + \frac{n\sigma}{a_i'\left(v_i'\right)^2}\right]\sinh 2a_i'v_i'\, dv_i'$$

where

$$\bar{u}_i = \left(\frac{8kT}{\pi m_i}\right)^{1/2}$$

$$a_i' = a_i\left(u_g'\right)^2$$

$$v_i' = \frac{u_i'}{u_g'}$$

Evaluation of this integral yields

$$\left(\overline{u'Q_d}\right)_i = \left(\pi r^2 \bar{u}_i\right) F_i$$

where

$$F_i = \frac{1}{2} \exp\left(-\frac{4U_i^2}{\pi}\right) + \frac{\pi}{8U_i}\left(1 + 2n\sigma + \frac{8U_i^2}{\pi}\right)\operatorname{erf}\left(\frac{2U_i}{\sqrt{\pi}}\right)$$

The functions $F_e = F_e\left(U_e\right)$ and $F_i = F_i\left(U_i\right)$ are shown in figure 1. Some useful limiting forms of the expressions for F_e and F_i are given in the following table where

$$K = \frac{1}{2} \exp - \frac{4U^2}{\pi} + \left(U + \frac{\pi}{8U}\right)\operatorname{erf} \frac{2U}{\sqrt{\pi}}$$

and

$$L = \frac{\pi}{4U} \operatorname{erf} \frac{2U}{\sqrt{\pi}}$$

TABLE III

LIMITING FORMS OF F_e and F_i

Condition	F_e	F_i
$U_e \gg 1$	U_e	U_i
$U_e \ll 1$	$\exp(-n\sigma)$	$K_i + L_i n\sigma$
$U_i \ll 1$	$\exp(-n\sigma)$	$1 + n\sigma$
$n = 0$	K_e	K_i
$U_e = U_i = n = 0$	1	1

The condition $n = 0$ corresponds to no charge on the drop. It has been shown in reference 15 that zero charge on particles (solid or liquid) can occur only under exceptional circumstances, for which thermionic emission and the electron and ion fluxes balance each other with no charge on the particle. The condition $U_e \gg 1$ corresponds to values of u_g' which are far too large to be of practical interest.

For all the remaining conditions $F_e = \exp(-n\sigma)$, just as it is for a probe at rest. For $U_i \ll 1$, the function F_i can be interpreted as an enhancement of the geometrical drop cross section πr^2 by the factor $1 + n\sigma$. However, as U_i increases to values which are large compared with unity, $\pi r^2 F_i$ approaches $\pi r^2 U_i$ instead of πr^2. It is more useful to consider F_i to be an enhancement factor for the product $\pi r^2 \bar{u}_i$. As figure 1 shows F_i sometimes has a minimum value near $U_i = 1$, but it always tends to become large and independent of n for $U_i \gg 1$.

The development of a sheath is necessary if the surface of the probe is to be at a different potential from the plasma, but its presence causes the influence of the electric field around the probe to be effectively limited to a distance from the probe surface of the order of the Debye length λ_D. Thus, if $r + \lambda_D < r\sqrt{1 + \frac{L_i n\sigma}{K_i}}$, the ion collection rate will be reduced from $\pi r^2 \bar{u}_i \left(K_i + L_i n\sigma\right)$ to $\pi \left(r + \lambda_D\right)^2 \bar{u}_i K_i$.

It is useful to consider the following expressions for the ion collection rate: If $\lambda_D \ll r$, the condition $1 + \frac{L_i n\sigma}{K_i} \geqq \left(1 + \frac{\lambda_D}{r}\right)^2$ holds, and the ion collection rate is $\pi r^2 \bar{u}_i K_i$. The sheath has negligible thickness; thus, the effective cross section of the drop for contact collision with ions is the same as if there were no sheath. If $\lambda_D \gg r$, the condition $1 + \frac{L_i n\sigma}{K_i} \leqq \left(1 + \frac{\lambda_D}{r}\right)^2$ holds and the ion collection rate is $\pi r^2 \bar{u}_i \left(K_i + L_i n\sigma\right)$. Figure 1 shows that, for the RAM B2 conditions, where U_i does not exceed about 3 and where $\mu \approx 235$, the value of $K_i + L_i n\sigma$ lies within the limits 3.80 to 4.87.

APPENDIX B

DIFFERENTIAL EQUATIONS FOR CHARGING PROCESS

Under the assumptions used in the derivation of equations (3) and (4), the only way in which electrons and ions can recombine is by collection of positive and negative charges on the surfaces of drops of radius r, upon which they neutralize each other. Conservation of charge requires that

$$c_i - c_e = nc_p \tag{B1}$$

By treating c_p as a constant, equations (3), (4), and (B1) can be rewritten as

$$\tau_e \dot{c}_e + c_e = 0 \tag{B2}$$

$$\tau_i \dot{c}_i + c_i = 0 \tag{B3}$$

$$\tau_e \dot{n} + n = \frac{c_i}{c_p}\left(1 - \frac{\tau_e}{\tau_i}\right) \tag{B4}$$

where

$$\tau_e = \left[\mu \pi r^2 c_p \bar{u}_i \exp(-n\sigma)\right]^{-1}$$

$$\tau_i = \left[\pi r^2 c_p \bar{u}_i \left(K_i + L_i n\sigma\right)\right]^{-1}$$

$$\mu = \left(\frac{m_i}{m_e}\right)^{1/2}$$

Equation (B4) is not an independent differential equation; it is simply a corollary equation which states explicitly the variation of the charge on the drops.

Since $\mu \gg 1$, $\tau_e \ll \tau_i$ in the initial part of the charging process, which begins with $n = 0$ at $t = 0$. It can be seen from equations (B2) to (B4) that $\dot{n}$ is initially positive and that it decreases until $\dot{n} = 0$, at which point $\tau_e c_i = \tau_i c_e$ and n has the value n_1, where n_1 is the solution of the transcendental equation

$$\left(1 - n_1 \frac{c_p}{c_i}\right)\left[\mu \exp(-n\sigma)\right] = K_i + L_i n_1 \sigma \tag{B5}$$

If $n_1 c_p \ll c_{e0}$, then $c_{i1} \approx c_{e1} \approx c_{e0}$, and equation (B5) becomes

$$\mu \exp(-n_2\sigma) \approx K_i + L_i n_2 \sigma \tag{B6}$$

Equation (B6) can also be obtained by setting $\tau_e = \tau_i$, which means that, if $n_1 c_p \ll c_{e0}$, equations (B2) to (B4) approach the following asymptotic forms when n approaches its peak value:

$$\tau^* \dot{c}_e + c_e = 0 \tag{B7}$$

$$\tau^* \dot{c}_i + c_i = 0 \tag{B8}$$

$$n = \frac{c_i}{c_p}\left(\frac{\tau_i - \tau_e}{\tau^*}\right) \tag{B9}$$

where $\tau^* \approx \tau_e \approx \tau_i$.

It can be seen from equation (B1) and the condition $\tau_e c_i = \tau_i c_e$ that τ_i must always be larger than τ_e, even though they are nearly equal when $n_1 c_p \ll c_{e0}$. The subsequent decrease in n is slow compared with the decreases in c_e and c_i. This condition is due to the fact that c_e and c_i are nearly equal and are decreasing at nearly the same rate. In fact, $n \approx n_2$ = Constant, as long as equation (B6) holds. The values of τ_e and τ_i diverge slowly as n decreases, and equations (B7) to (B9) are not valid when c_i decreases enough to make nc_p no longer negligible compared with c_i. However, the decrease in n is still slow. The effect of a shorter time constant for the decay of c_e is compensated by the effect of c_e being smaller than c_i; thus, approximate equality is maintained between $\dot{c}_e$ and $\dot{c}_i$.

These equations describe the effects of adding droplets to an over-ionized plasma. There is an initial rapid rise of negative charge on the drops to a value which never exceeds the value $-n_2 e$ and which, in general, is $-n_1 e$. The charge on the drops remains almost constant after it reaches the peak value but does decrease slowly with time. The ion concentration is practically unchanged during the short charging period and then decreases with time. The same is true for the electron concentration, except that it is not always possible to neglect the loss of the electrons used to charge the drops.

An additional restriction on the value of n is that it must not exceed n_m, the maximum number of electrons which the drop can absorb without being disrupted by electrostatic repulsion forces. It is shown in appendix D that $n < n_m$ for any physically realizable water drop.

APPENDIX B

Discussion of Special Forms of the Rate Equations

Except under special circumstances, solutions of equations (B2) to (B4) must be obtained by numerical integration. However, valid approximate forms of the equations have been found for the conditions of interest in this report and are designated as case I and case II.

Case I.- For case I, the drop-charging process has negligible effect on c_e $\left(nc_p \ll c_{e0}\right.$ and $c_i = c_{e0}$, when n approaches $\left.n_2\right)$. The details of the charging process are immaterial since neither c_e nor c_i changes appreciably while the drop is charging. Therefore, equations (B2) to (B4) approach the asymptotic forms given by equations (B7) to (B9). The initial conditions are at $t = 0$, $c_e = c_i = c_{e0}$, and $n = n_2$. When c_i decreases enough to assure that $n_2c_p \ll c_i$ is no longer a good approximation, the solution can be continued with equations of the same form as those used in case II.

Case II.- For case II, a correction is required for effect on c_e of drop-charging process $\left(\text{that is, } nc_p \approx c_{e0} \text{ and } c_i = c_{e0} \text{ when } n \text{ approaches } n_1\right)$. The details of the charging process are uninteresting for this case also. The remaining changes in c_i, c_e, and n are given by equations (B2) to (B4) with the initial conditions at $t = 0$, $c_i = c_{e0}$, $c_e = c_{e0} - n_1c_p$, and $n = n_1$. Since $\dot{c}_e \approx \dot{c}_i$ after n reaches the value n_1, a good approximate solution is obtained by setting $\dot{n} = 0$ so that equations (B2) to (B4) become

$$\tau_e\dot{c}_e + c_e = 0$$

$$\tau_i\dot{c}_i + c_i = 0$$

$$n = n_1$$

These equations become invalid when the condition $n_1c_p \approx c_i - c_e$ is violated.

APPENDIX C

APPROXIMATE TREATMENT OF GAS DYNAMICS AND THERMODYNAMICS

Conservation of mass along a stream tube requires that

$$\rho_g u_g'' A = \rho_{g3} u_{g3}'' A_3$$

and

$$c_p u_p'' A = c_{p3} u_{p3}'' A_3$$

where it is assumed that stream tube area changes slowly enough to enable drop paths to follow the flow stream tubes.

Conservation of momentum along a stream tube requires that

$$pA + \left(\rho_g u_g'' A\right) u_g'' + \left(\frac{4}{3}\pi r^3 \rho_W c_p u_p'' A\right) u_p'' = p_3 A_3 + \left(\rho_{g3} u_{g3}'' A_3\right) u_{g3}'' + \left(\frac{4}{3}\pi r^3 \rho_W c_{p3} u_{p3}'' A_3\right) u_{p3}''$$

By dropping the pressure terms, this equation can be reduced to the simple relationship

$$u_g'' + M^* u_p'' = u_{g3}'' + M^* u_{p3}'' \tag{C1}$$

The equation of motion for a drop which is moving parallel to the direction of gas flow under conditions such that the mean free path of a gas molecule is large compared with the drop diameter is

$$\frac{4}{3}\pi r^3 \rho_W u_p'' \frac{du_p''}{dx} = \pi r^2 \rho_g \left(u_g'' - u_p''\right)^2 \tag{C2}$$

where it is assumed that the drag coefficient is equal to 2.

The approximate analysis of water droplet acceleration which is used in this report is based on the assumptions that pressure, density, and temperature in the plasma do not change when water is added and that the drops have constant acceleration equal to the initial acceleration until the drops are moving at the same speed as the plasma. Since, by equation (C2), the force on a drop vanishes for $u_g'' = u_p''$, the limiting value for u_p'' and u_g'' is calculated from equation (C1) to be

$$u''_{p4} = u''_{g4} = \frac{u''_{g3} + M^{*}u''_{p3}}{1 + M^{*}}$$

Figure 10 shows how the velocity, temperature, density, and distance traveled by a drop computed by using the approximations mentioned compare with the same quantities obtained from the machine program described in reference 21. The machine computation was carried out with a frozen-gas composition representative of the flight case instead of using an equilibrium gas composition as described in reference 21.

The machine computations included some of the same assumptions used in this paper. For example, pressure was assumed to be constant along the stream tube, drop size was taken to be uniform, and the water was assumed to be distributed uniformly in the shock layer. However, the effects of heat transfer and evaporation were calculated, and the drag coefficient was determined as a function of local Mach number and Reynolds number.

APPENDIX D

DEMONSTRATION THAT n IS LESS THAN n_m FOR ANY PHYSICALLY REALIZABLE WATER DROP

The maximum charge that can be carried by a liquid drop without breaking up because of electrostatic repulsion between its parts can be found as follows: By definition, the coefficient of surface tension γ is the rate of increase of surface energy with surface area. In mathematical terms, this relation can be written for a spherical surface as

$$\frac{dW}{dr} = 8\gamma\pi r$$

The limiting condition for stability of a spherical surface when surface tension forces are opposed by electrical forces is given by equating this expression to the rate of change of electrostatic energy with radius. The result is

$$n_m = \frac{4\pi r\sqrt{2\gamma\epsilon_o r}}{e}$$

From the definition of σ

$$n = n\sigma\,\frac{4\pi\epsilon_o rkT}{e^2}$$

Thus,

$$\frac{n}{n_m} = \left(\frac{R}{r}\right)^{1/2}$$

where

$$R = (n\sigma)^2\left(\frac{kT}{e}\right)^2\frac{\epsilon_o}{2\gamma}$$

On the basis of this criterion, it is expected that for $r \leqq R$, a water drop will break up before it acquires n electron charges, but for $r > R$, it will not. The length R thus represents a minimum radius for drops in the problem being considered. By using $T = 2600^{\circ}$ K, $n\sigma = 4$, and $\gamma = 7 \times 10^{-2}\,\mathrm{Nm}^{-1}$, a typical value of R is found to be of the order of 10^{-10} m. Since the diameter of a single water molecule is also of order 10^{-10} m, the small calculated value of R means that every physically realizable drop of water will be stable against disruption by electrostatic forces under the conditions of the problem under consideration.

REFERENCES

1. Cuddihy, William F.; Beckwith, Ivan E.; and Schroeder, Lyle C.: RAM B2 Flight Test of a Method for Reducing Radio Attenuation During Hypersonic Reentry. NASA TM X-902, 1963.

2. Cuddihy, W. F.; and Hughes, J. Kendrick: Simulated Reentry Tests of a Method for Reducing Radio Blackout by Material Addition to the Ionized Flow Field. NASA TM X-988, 1964.

3. Kuhns, Perry W.; and Cooper, Dale W.: Effect of Water Addition on Microwave Transmission Through a Cold Plasma Layer. NASA TM X-874, 1963.

4. Spencer, Dwain F.: An Evaluation of the Communication Blackout Problem for a Blunt Mars-Entry Capsule and a Potential Method for the Elimination of Blackout. Tech. Rept. No. 32-594 (Contract No. NAS 7-100), Jet Propulsion Lab., C.I.T., Apr. 15, 1964.

5. Soo, S. L.: Gas-Solid Suspensions at High Temperatures. J. Appl. Phys., vol. 34, no. 6, June 1963, pp. 1689-1696.

6. Rosen, Gerald: Method for the Removal of Free Electrons in a Plasma. Phys. of Fluids (Res. Notes), vol. 5, no. 6, June 1962, pp. 737-738.

7. Einbinder, Harvey: Generalized Equations for the Ionization of Solid Particles. J. Chem. Phys., vol. 26, no. 4, Apr. 1957, pp. 948-953.

8. Smith, Felix T.: On the Ionization of Solid Particles. J. Chem. Phys. (Letters to the Editor), vol. 28, no. 3, Mar. 1958, pp. 746-747.

9. Sodha, M. S.: Thermal and Photoelectric Ionization of Solid Particles. Brit. J. Appl. Phys., vol. 14, no. 4, Apr. 1963, pp. 172-176.

10. Arshinov, A. A.; and Musin, A. K.: Equilibrium Ionization of Particles. Rep. Acad. Sci. (USSR), vol. 118, no. 4, 1958, p. 747. (Also Soviet Physics "Doklady," vol. 3, May-June 1958, pp. 588-592.)

11. Spokes, G. Neil: The Role of Aluminum and Its Oxides as Sources or Moderators of Electrons in Solid Propellant Rocket Exhausts. 6th Quarterly Status Report (Contract AF-04(694)-128), Stanford Res. Inst., 1963. (Available as AD 434699.)

12. Soo, S. L.; and Dimick, R. C.: Experimental Study of Thermal Electrification of a Gas-Solid System. Proc. Winter Annual Meeting ASME, Nov. 1963, pp. 43-46.

13. Dimick, R. C.; and Soo, S. L.: Scattering of Electrons and Ions by Dust Particles in a Gas. Rept. Ill-14-P (AD-433862), Proj. SQUID Tech. (Contract Nonr 3623(00)), Univ. Illinois, Mar. 1964.

14. Soo, S. L.; and Dimick, R. C.: Interaction of Solid Particles With an Ionized Gas. Rept. Ill-12-P (AD-424859), Proj. SQUID Tech. (Contract Nonr 3623(00)), Univ. Illinois, Nov. 1963.

15. Kurzius, Shelby C.; and Skinner, R. E.: Effect of Solid Particles on Electron Concentrations in a Plasma. TP-72b (Contract AF 30(602)3142), AeroChem Res. Labs., Inc., Mar. 1964.

16. Beckwith, Ivan E.; and Huffman, Jarrett K.: Injection and Distribution of Liquids in the Flow Fields of Blunt Shapes at Hypersonic Speeds. NASA TM X-989, 1964.

17. Ingebo, Robert D.: Penetration of Drops Into High-Velocity Airstreams. Proc. NASA Conf. Communicating Through Plasmas of Atmospheric Entry and Rocket Exhaust. NASA SP-52, 1964, pp. 95-104.

18. Clark, Bruce J.: Breakup of a Liquid Jet in a Transverse Flow of Gas. NASA TN D-2424, 1964.

19. Green, H. L.; and Lane, W. R.: Particulate Clouds: Dusts, Smokes and Mists. Second Ed., E. & F. N. Spon Ltd., c.1964.

20. Fuchs, N. A.: The Mechanics of Aerosols. The MacMillan Company, c.1964.

21. Cuddihy, W. F.; Beckwith, I. E.; and Schroeder, L. C.: A Solution to the Problem of Communications Blackout of Hypersonic Reentry Vehicles. AMRAC Proceedings, Vol. IX, Pt. II, Inst. Sci. Technol., Univ. of Michigan, 1963, pp. 187-231. (Available from DDC as AD 344 601(4613-59-X, pt. II).)

22. Loeb, Leonard B.: Basic Processes of Gaseous Electronics. Univ. of California Press, 1955.

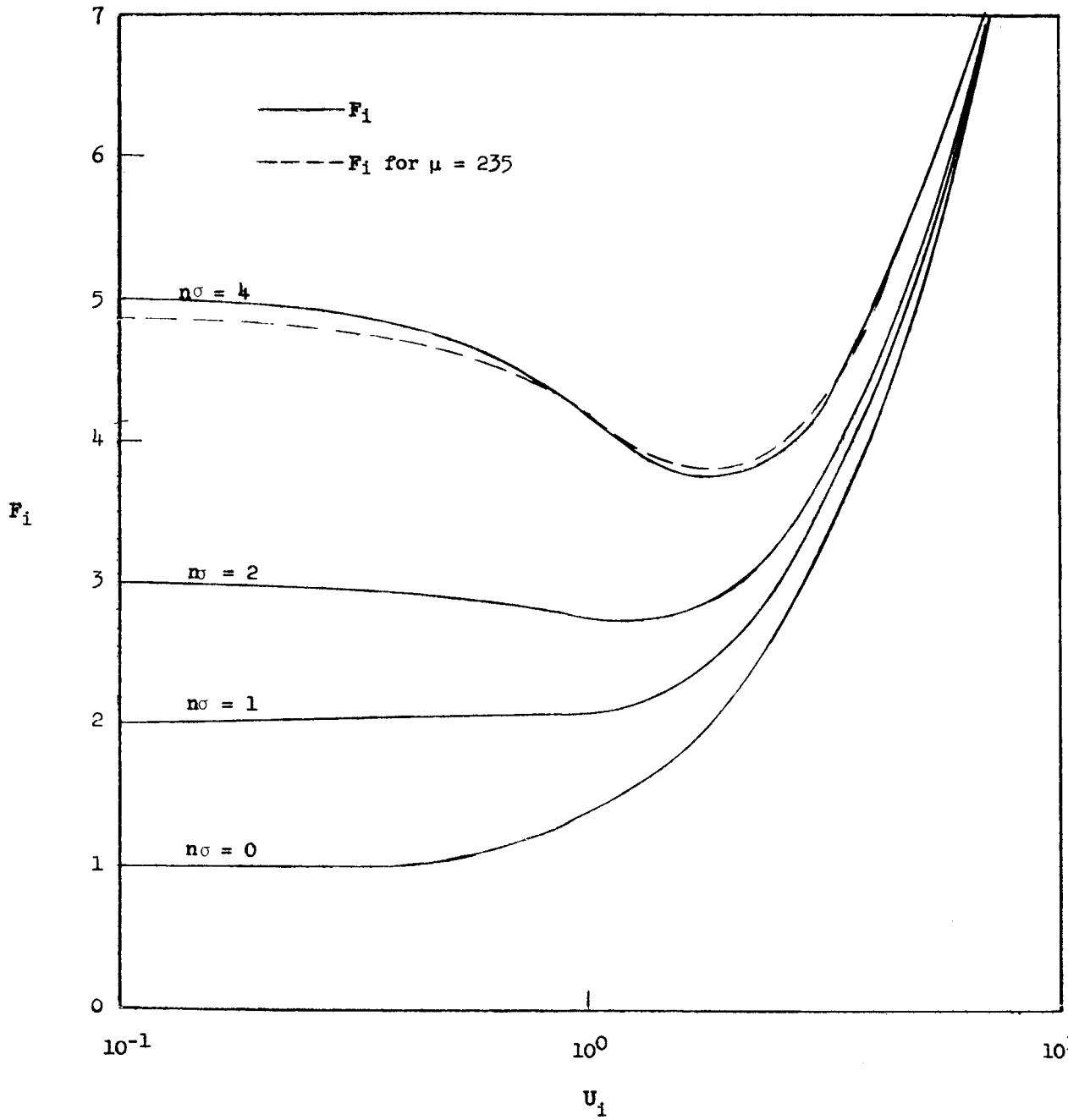

(a) F for ions.

Figure 1.- Variation of F with U.

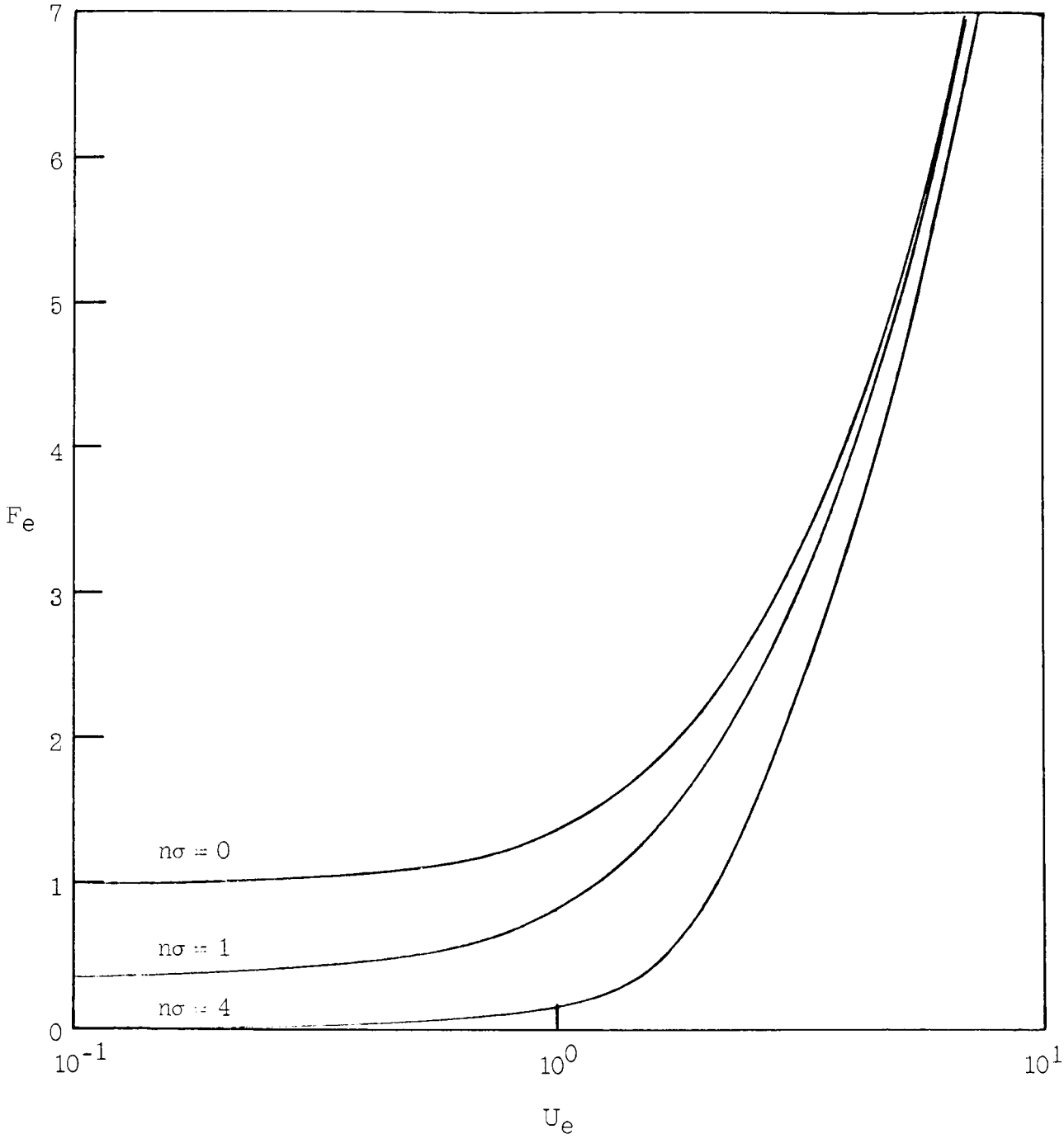

(b) F for electrons.

Figure 1.- Concluded.

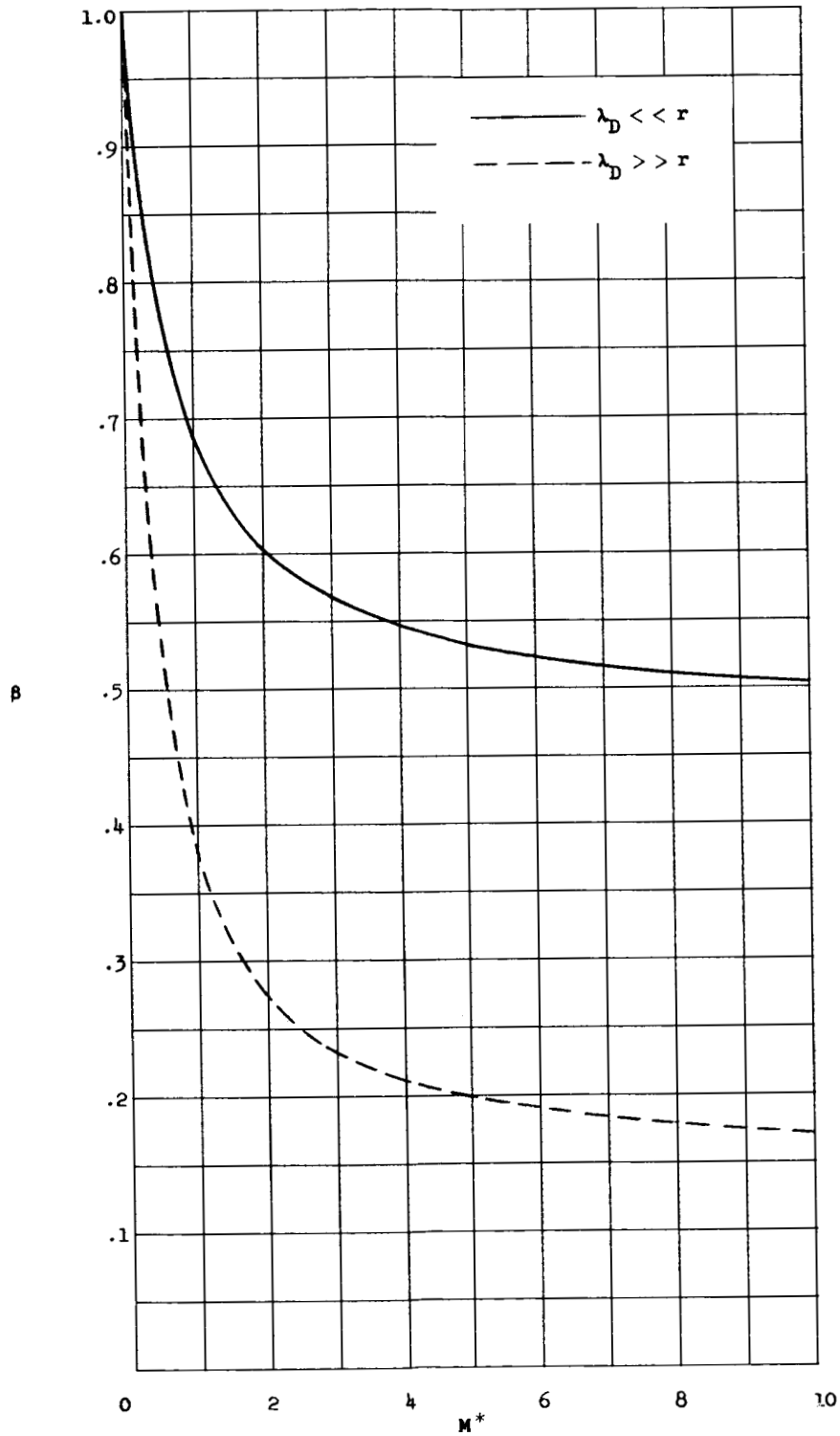

Figure 2.- Variation of β with M^*.

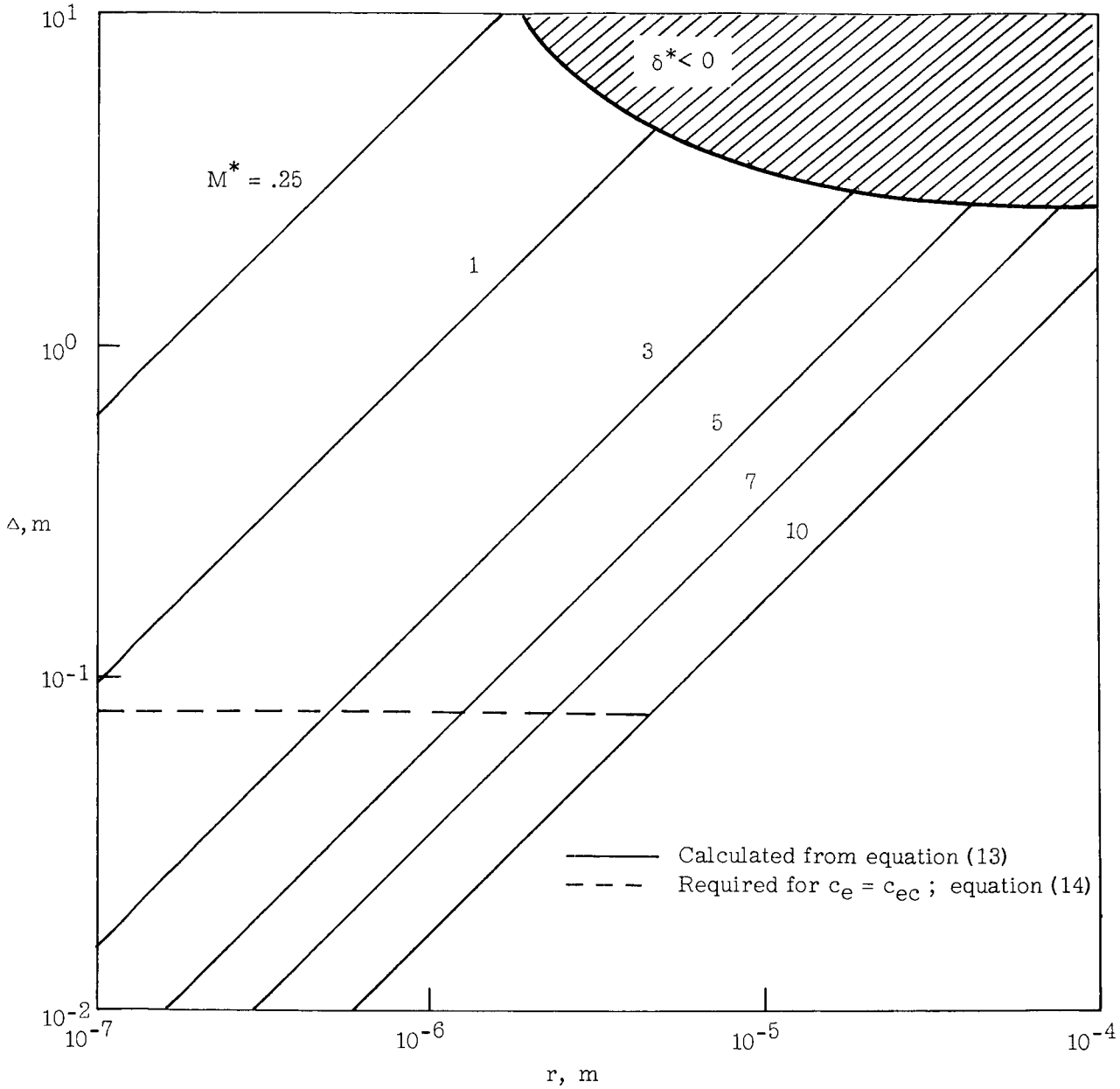

(a) Altitude, 4.78×10^4 m (157,000 ft).

Figure 3.- Variation of Δ with r and M*. $\lambda_D \ll r$.

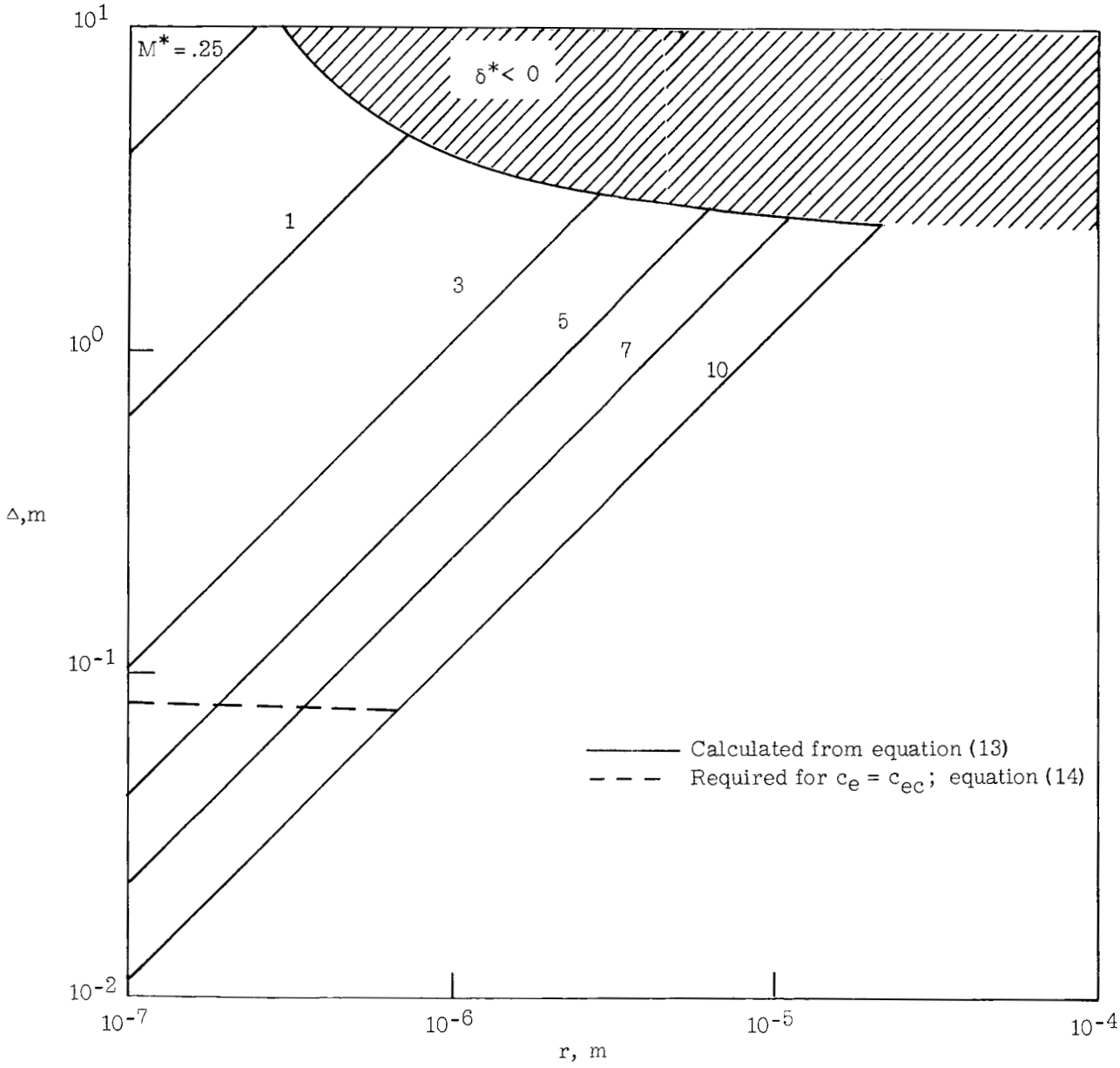

(b) Altitude, 6.40×10^4 m (210,000 ft).

Figure 3.- Concluded.

[redacted]
UNCLASSIFIED

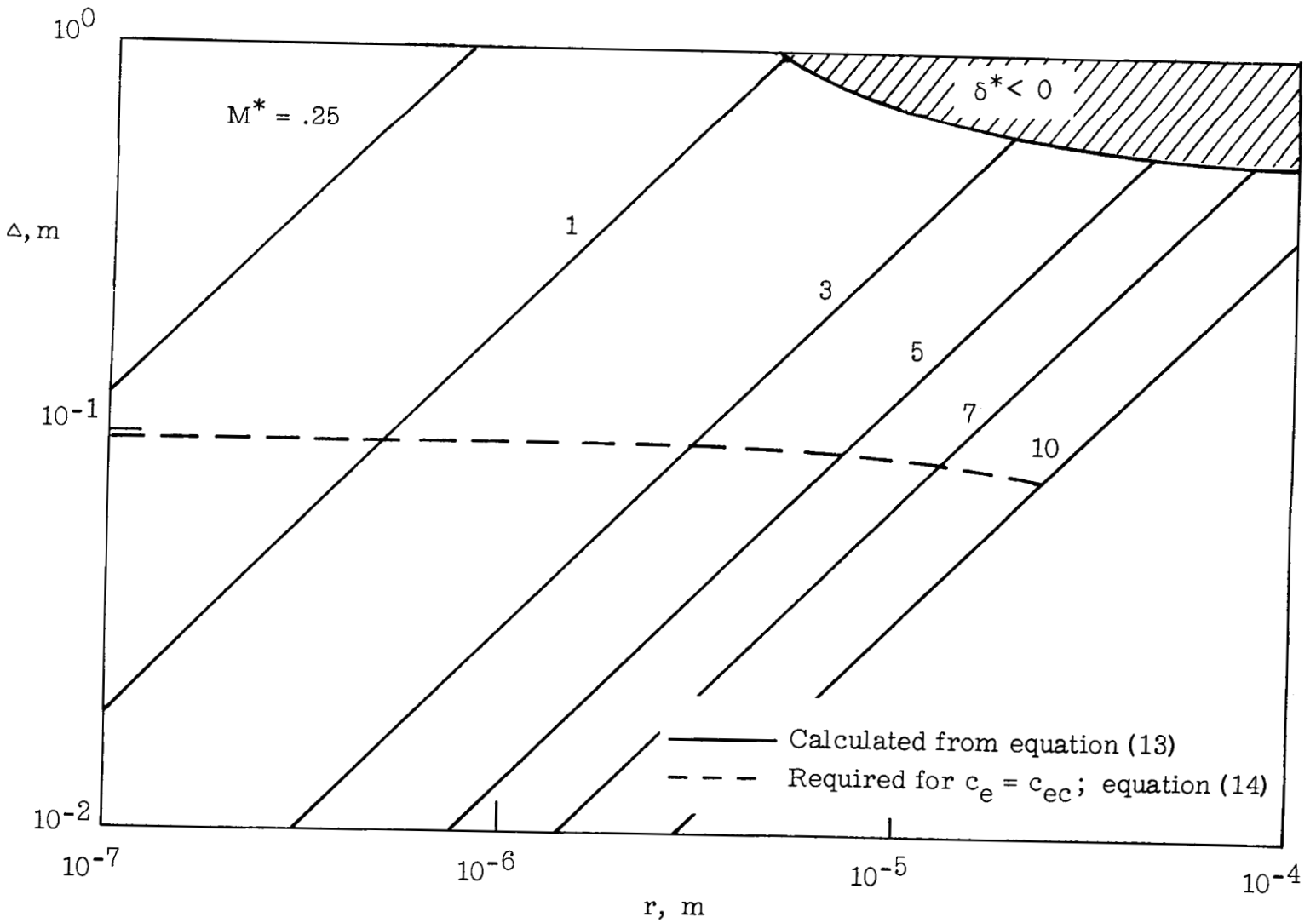

(a) Altitude, 4.78×10^4 m (157,000 ft).

Figure 4.- Variation of Δ with r and M^*. $\lambda_D \gg r$.

UNCLASSIFIED
[redacted]

UNCLASSIFIED

[redacted]

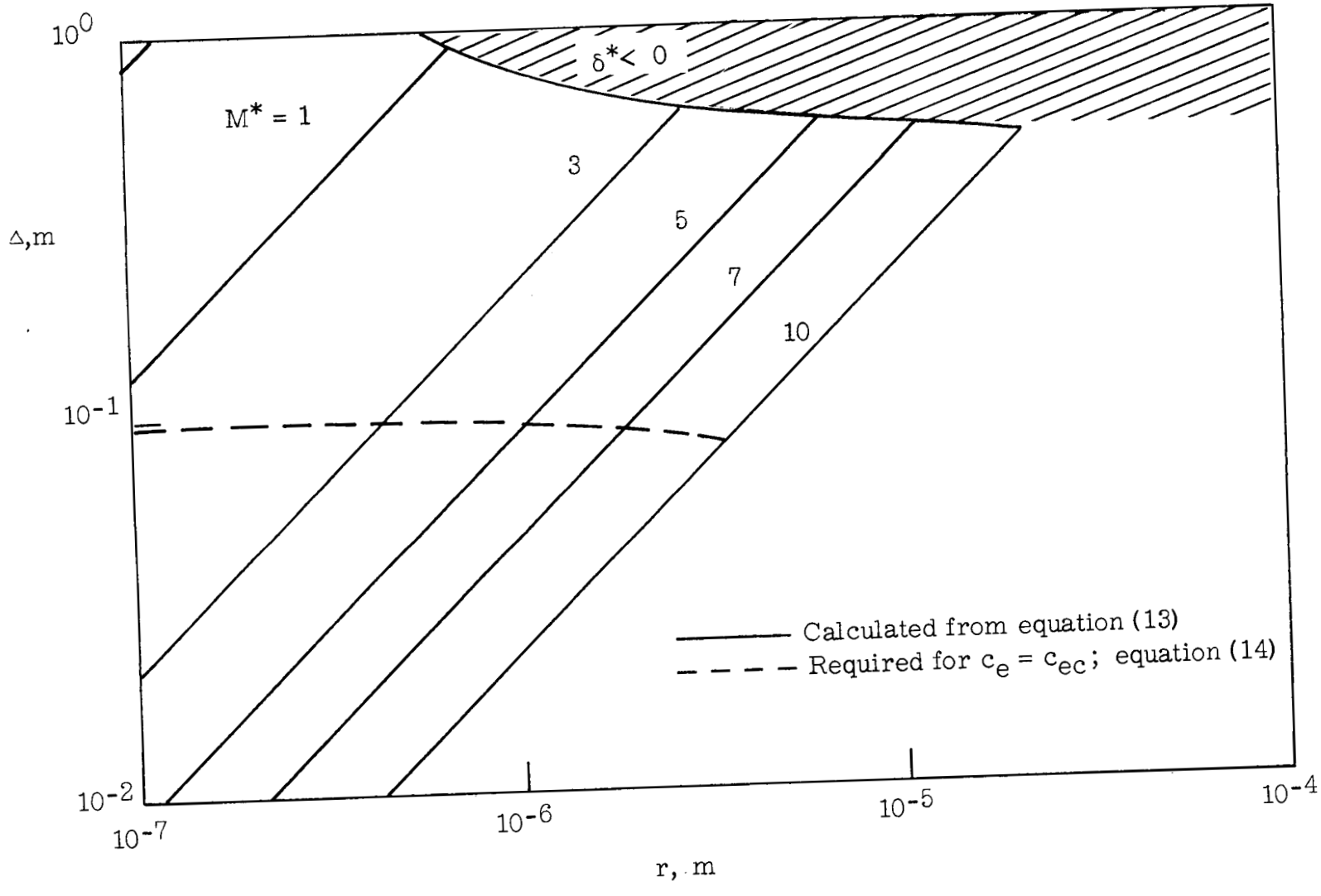

(b) Altitude, 6.40×10^4 m (210,000 ft).

Figure 4.- Concluded.

[redacted]

UNCLASSIFIED

[redacted]

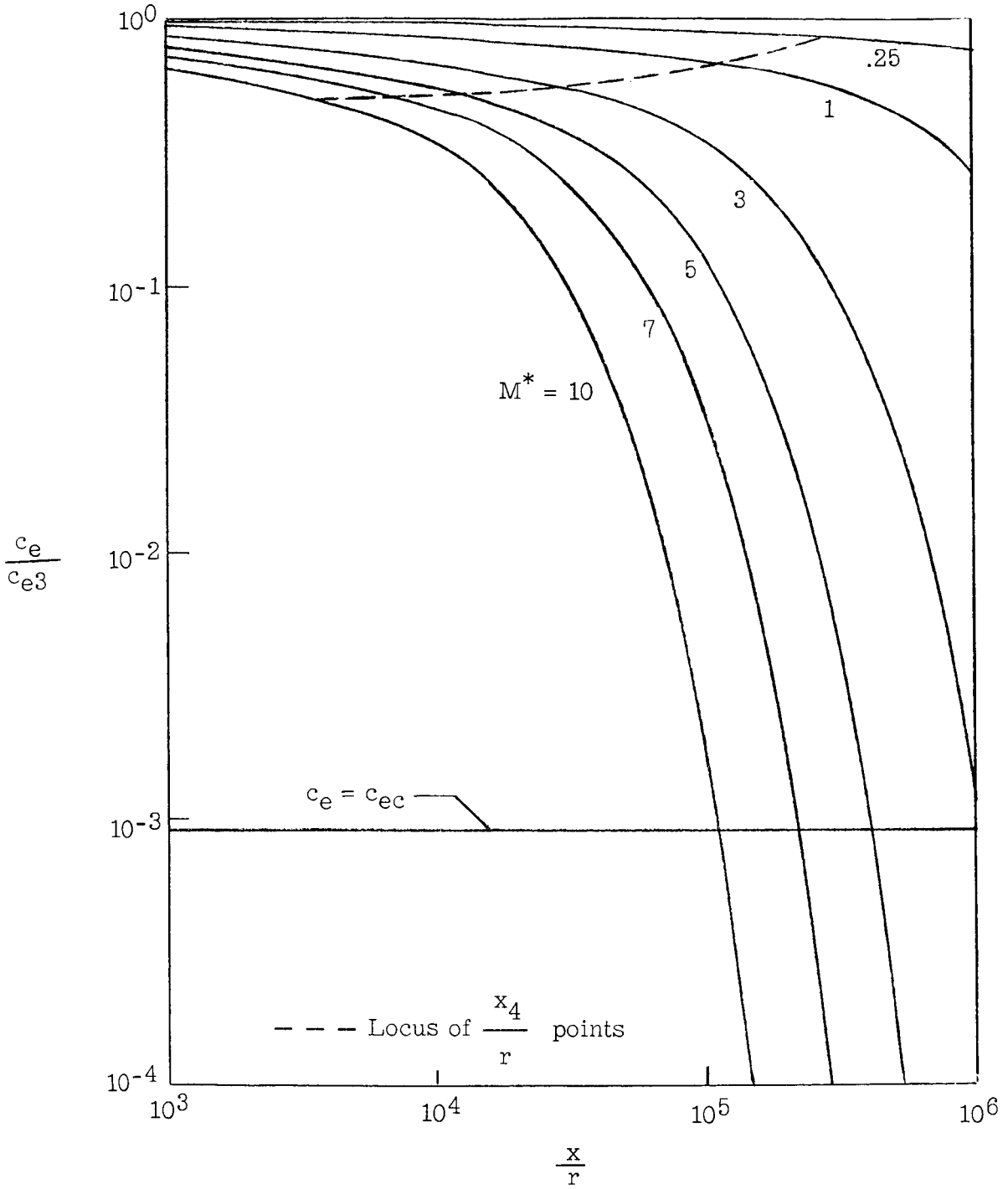

(a) Altitude, 4.78×10^4 m (157,000 ft).

Figure 5.- Reduction of c_e as a function of $\frac{x}{r}$ and M^*. $\lambda_D \ll r$.

[redacted]

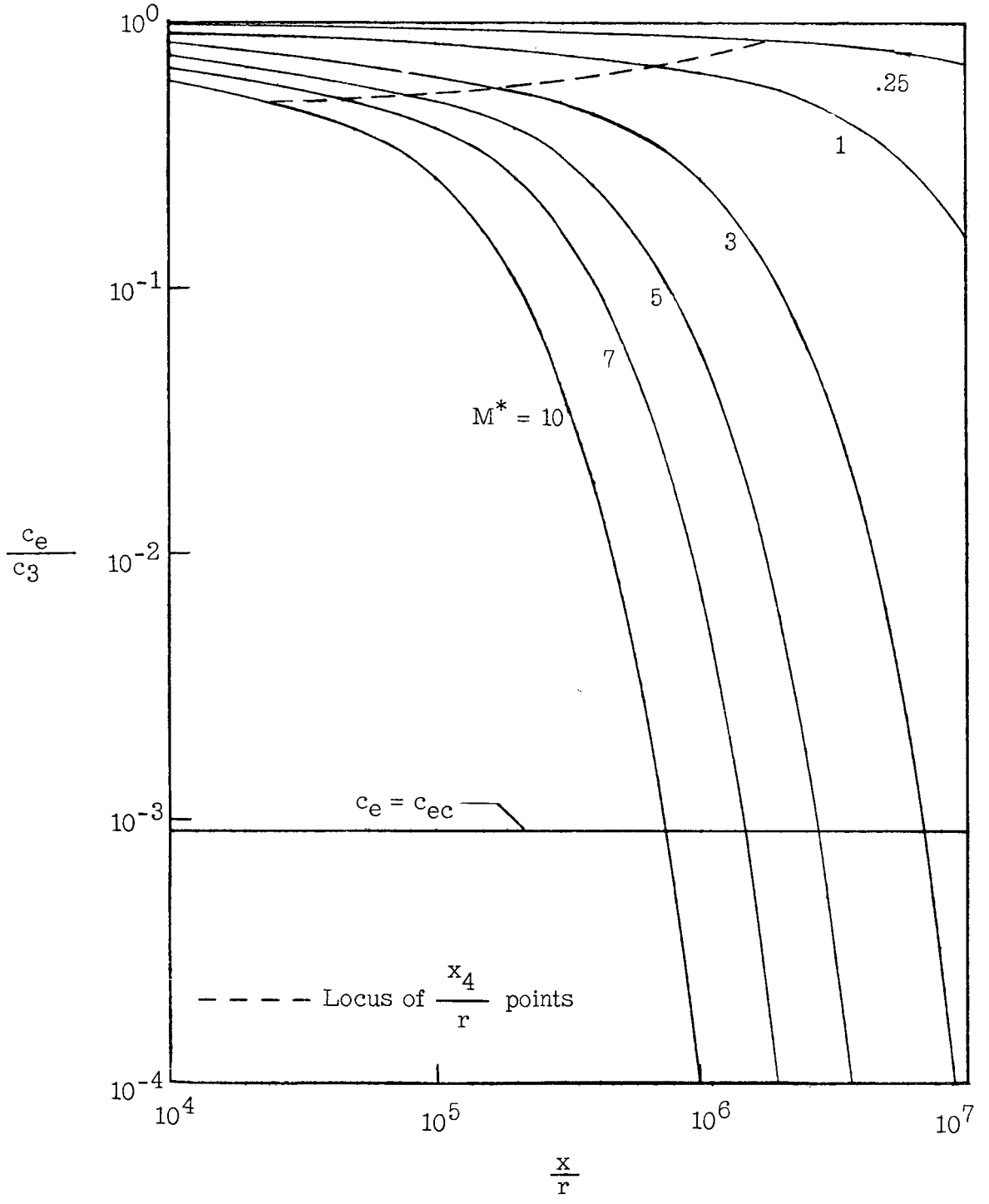

(b) Altitude, 6.40×10^4 m (210,000 ft).

Figure 5.- Concluded.

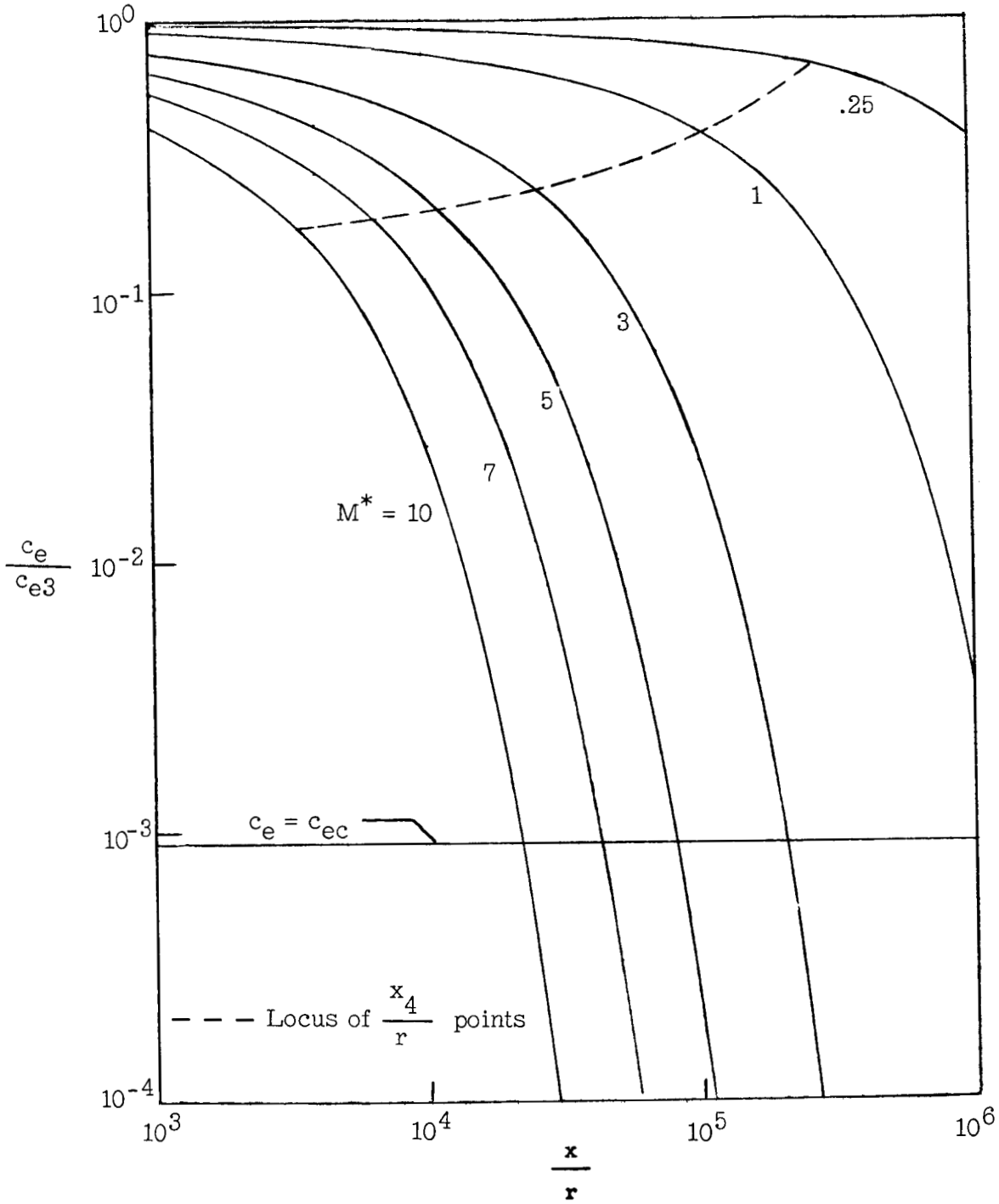

(a) Altitude, 4.78×10^4 m (157,000 ft).

Figure 6.- Reduction of c_e as a function of $\frac{x}{r}$ and M^*. $\lambda_D \gg r$.

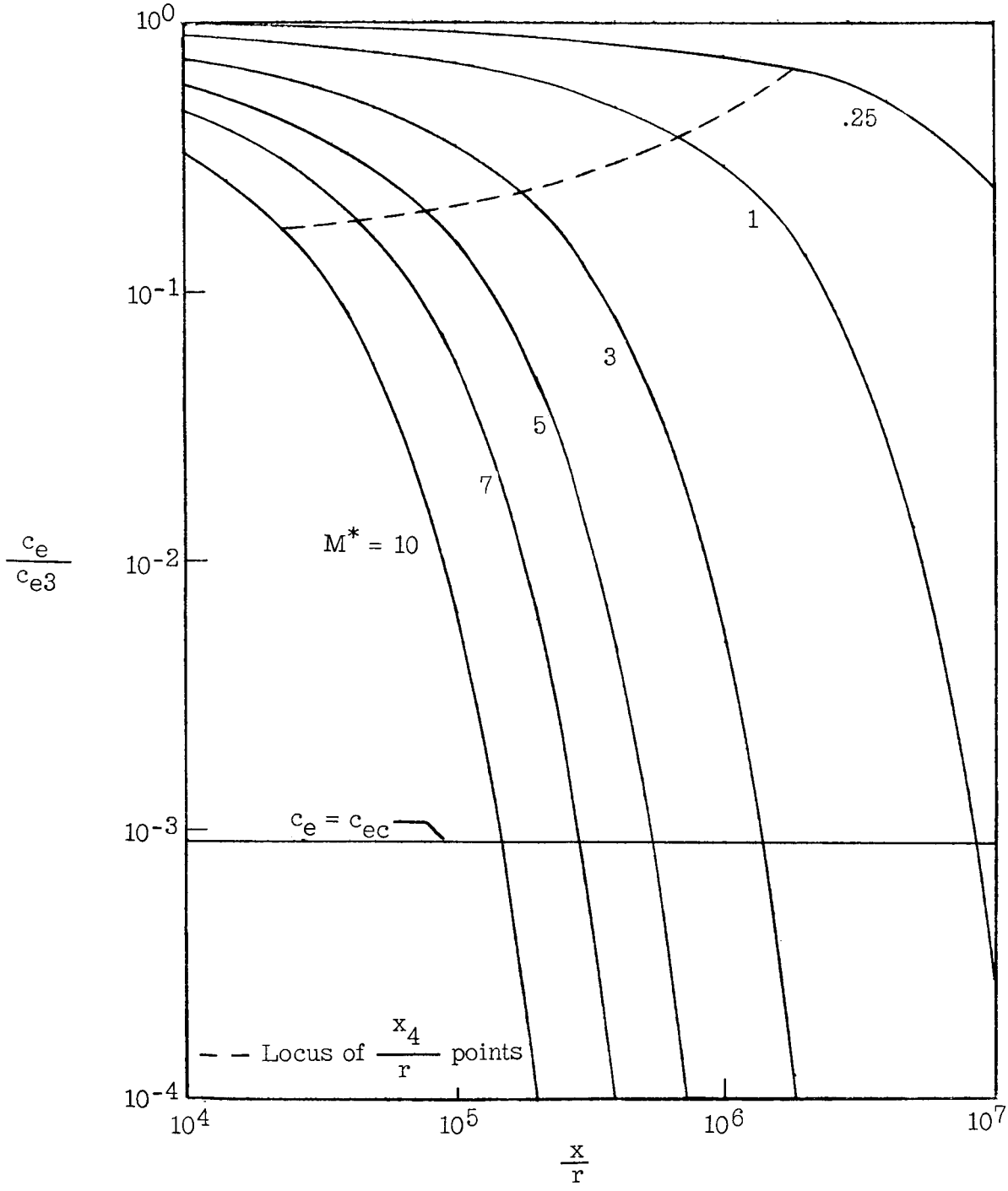

(b) Altitude, 6.40×10^4 m (210,000 ft).

Figure 6.- Concluded.

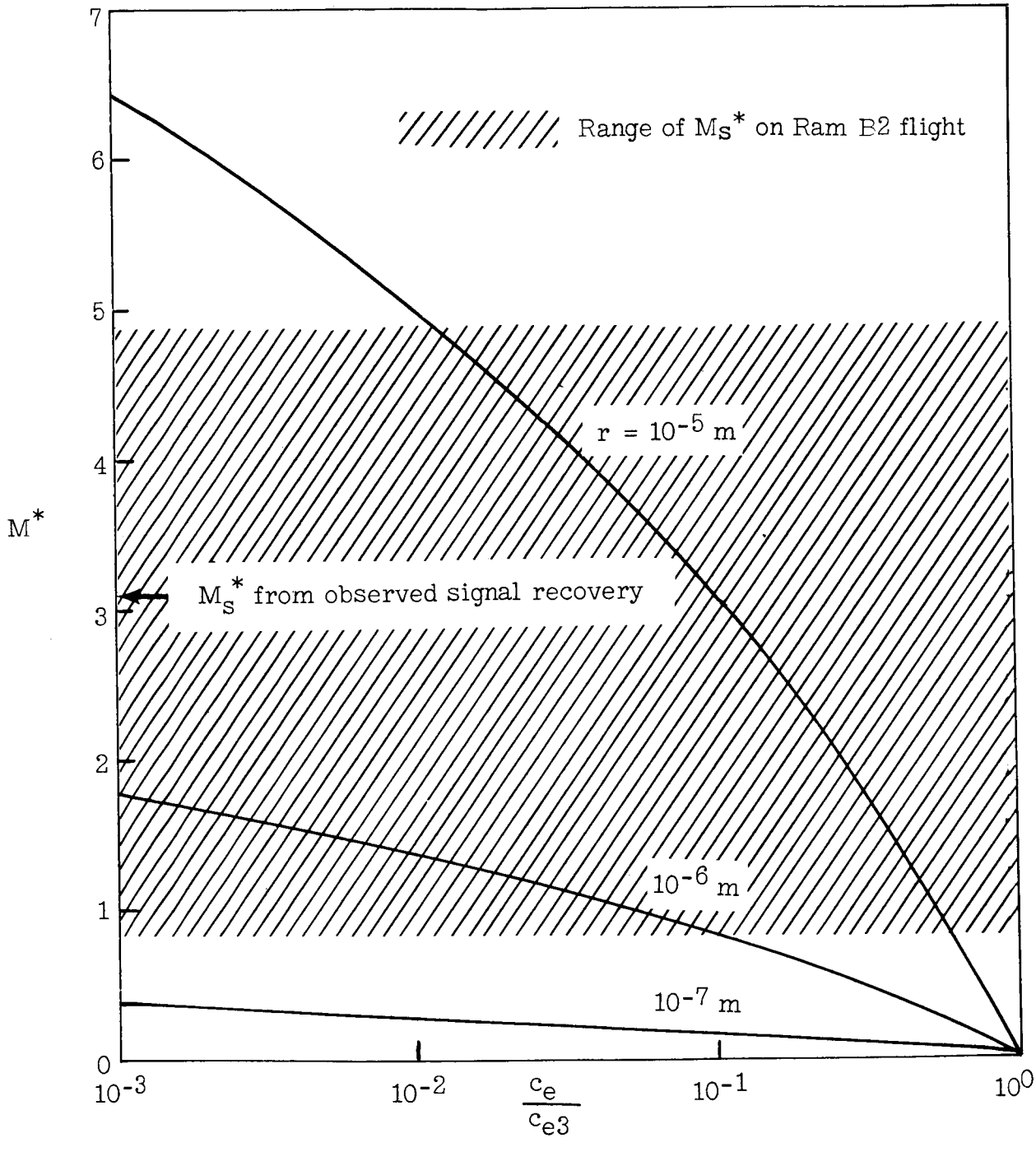

(a) Altitude, 4.78×10^4 m (157,000 ft).

Figure 7.- Mass flow ratio as a function of required reduction in electron concentration.

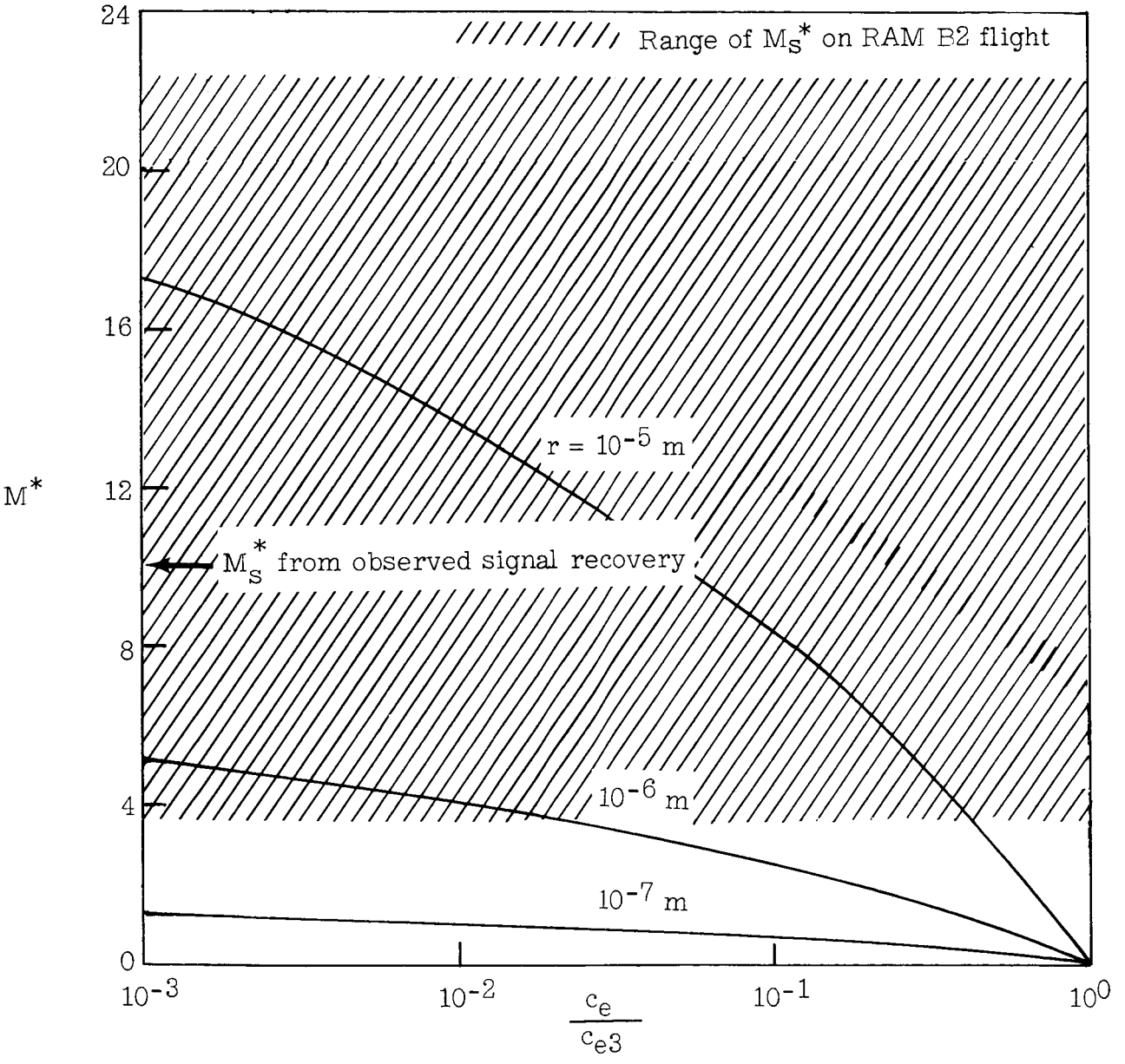

(b) Altitude, 6.40×10^4 m (210,000 ft).

Figure 7.- Concluded.

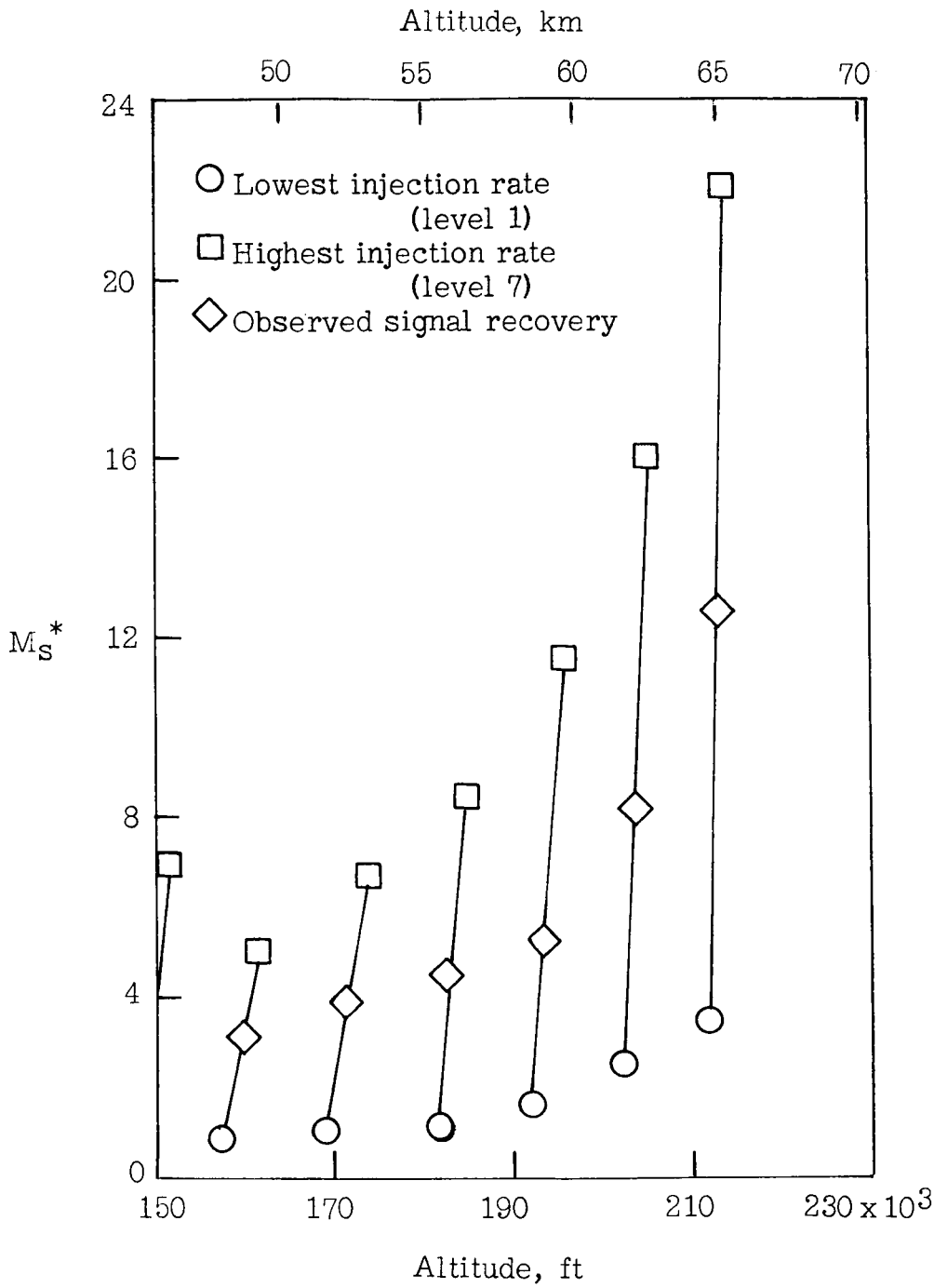

Figure 8.- Variation of M_s^* with altitude on RAM B2 flight.

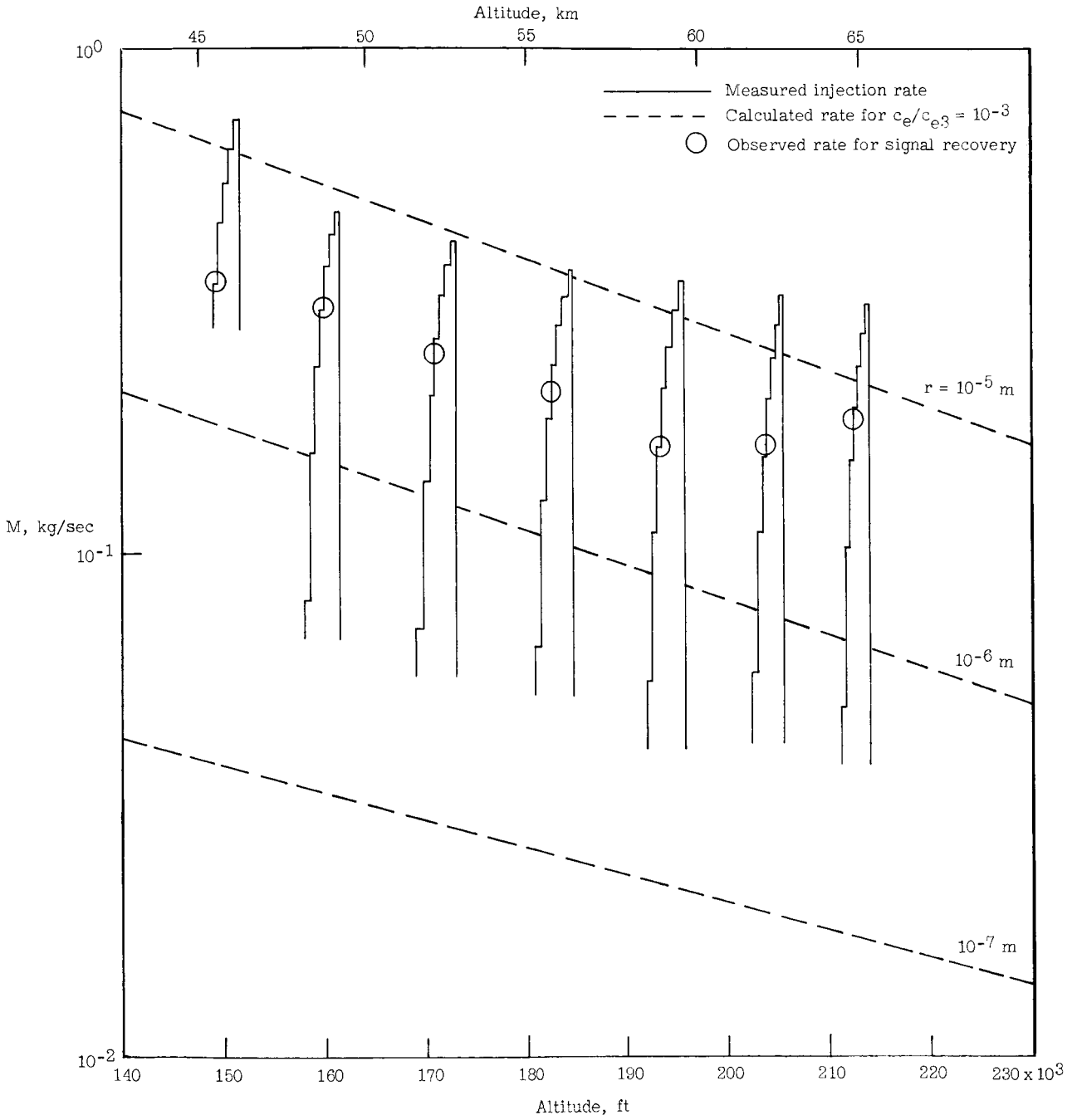

Figure 9.- Injection rate to reduce c_e to c_{ec} on RAM B2 flight.

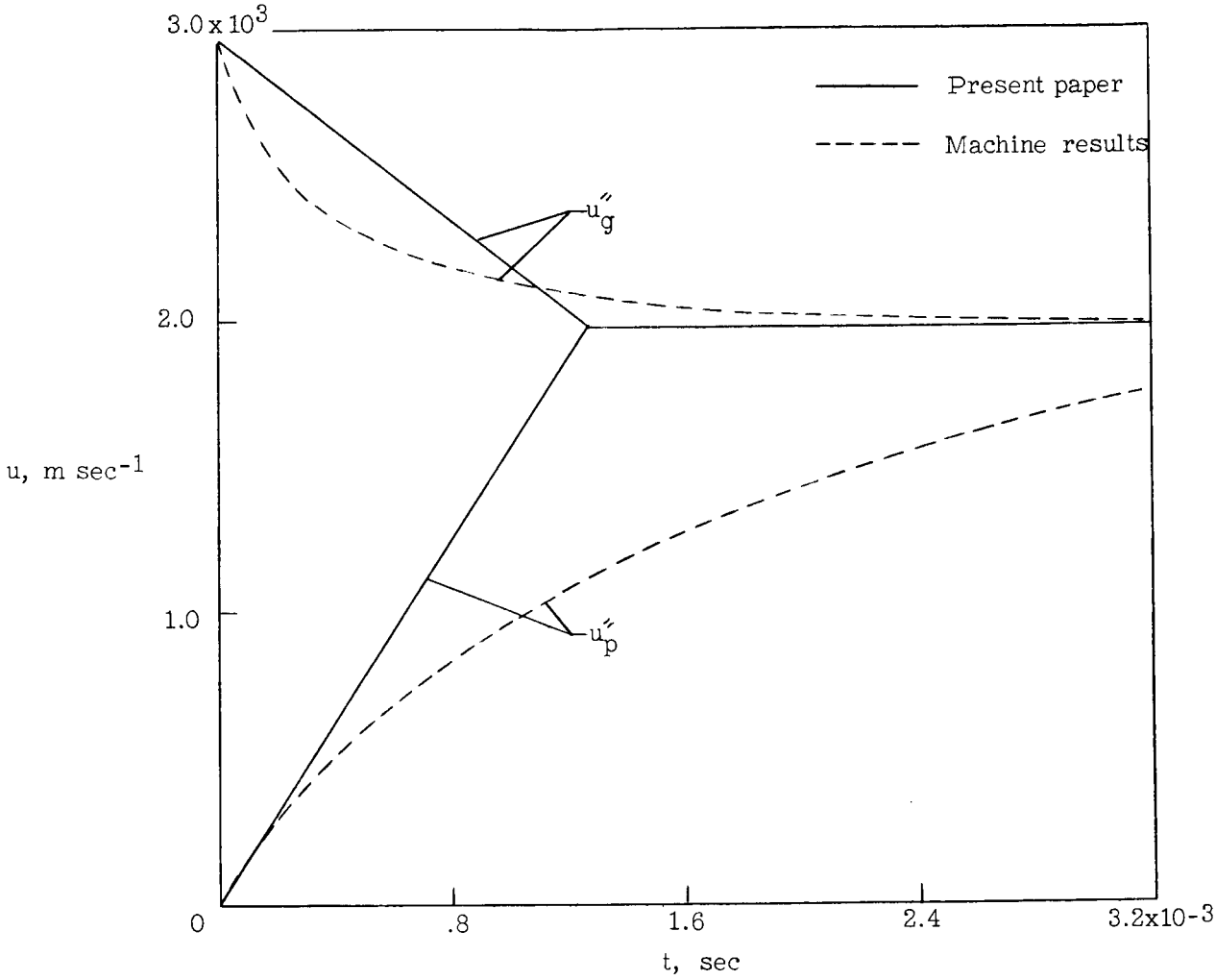

(a) Gas and drop velocities.

Figure 10.- Comparison of velocity, distance, temperature, and density as computed by approximate method used in this report with values computed by using an electronic data processing machine. Altitude, 4.78×10^4 m (157,000 ft); $M^* = 0.5$; $r = 6.74 \times 10^{-6}$ m.

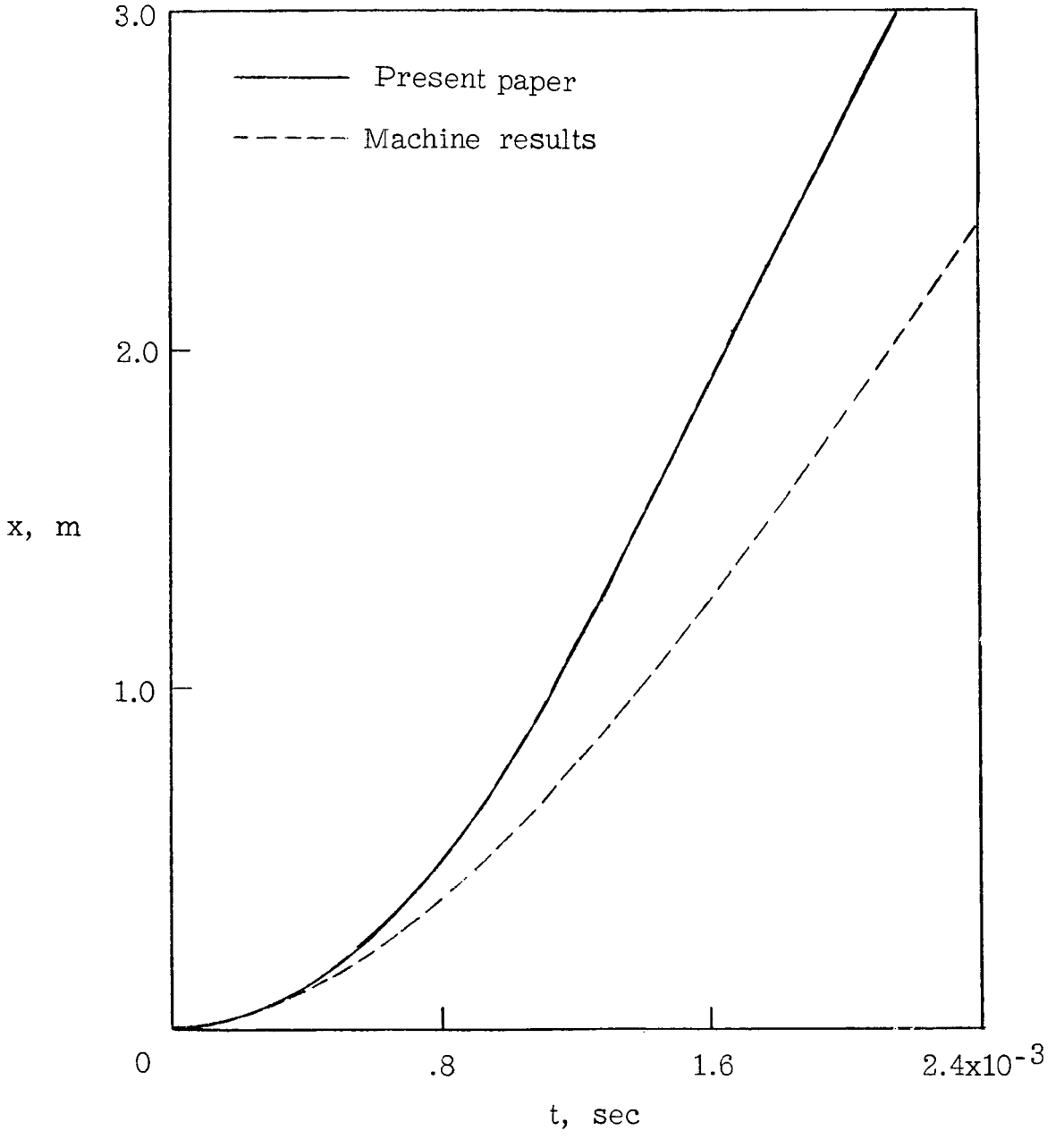

(b) Distance of drop from injection point.

Figure 10.- Continued.

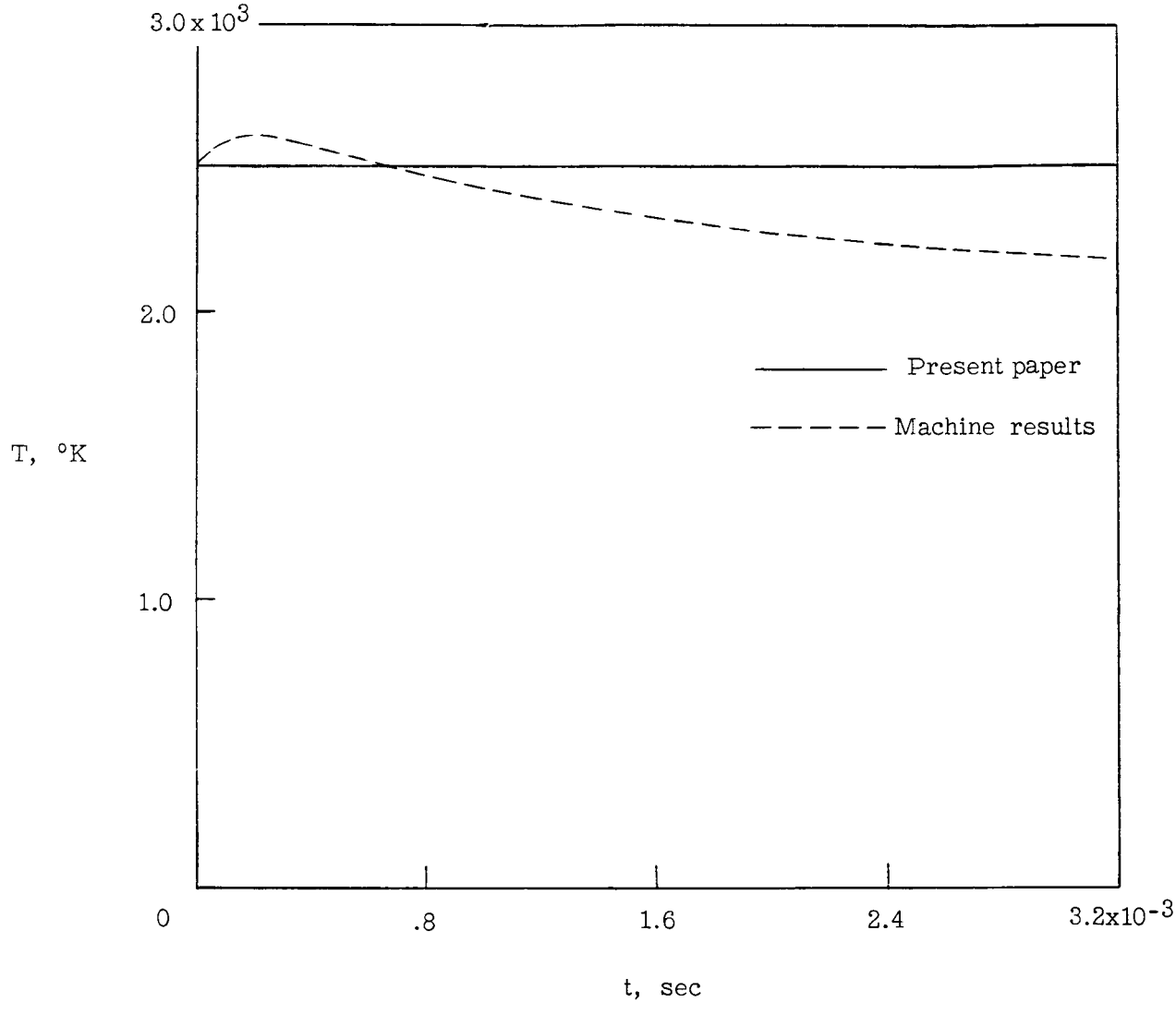

(c) Gas temperature.

Figure 10.- Continued.

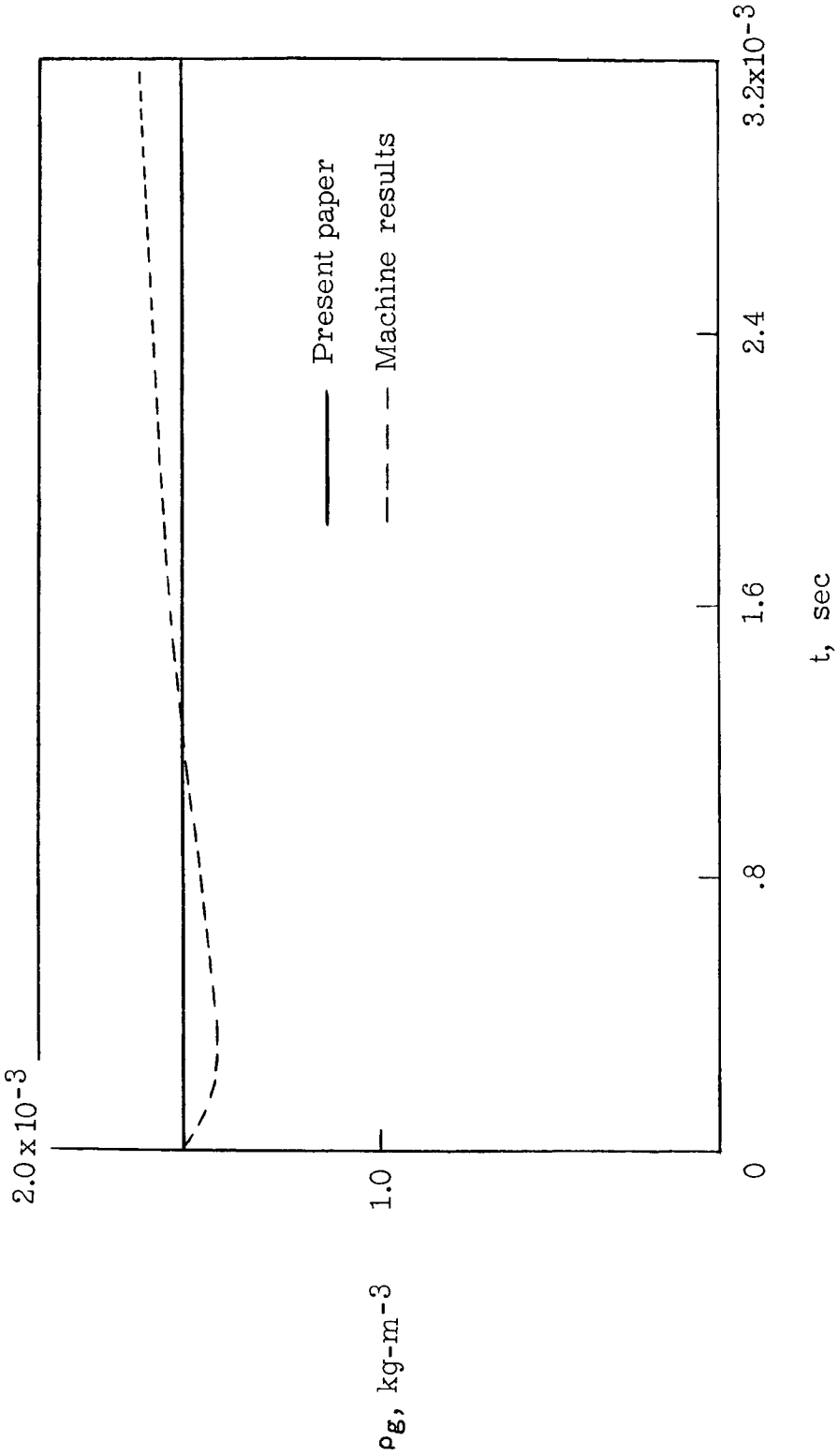

(d) Gas density.

Figure 10.- Concluded.

[redacted]
UNCLASSIFIED

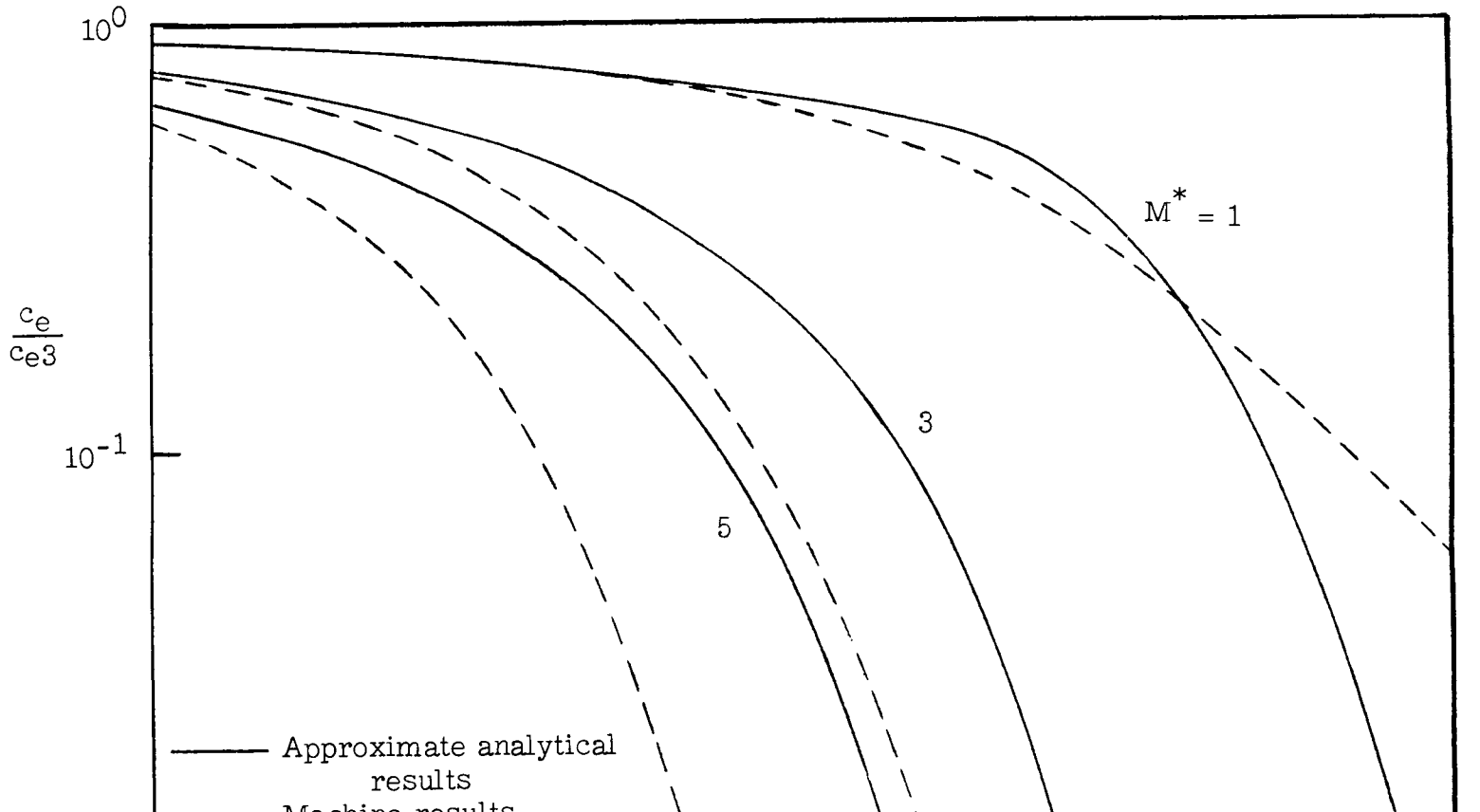

(a) $\frac{c_e}{c_{e3}}$ plotted against $\frac{x}{r}$.

Figure 11.- Comparison of analytical and machine solutions for electron decay. Altitude, 4.78×10^4 m (157,000 ft); drop radius, 10^{-6} m.

[redacted]
UNCLASSIFIED

UNCLASSIFIED

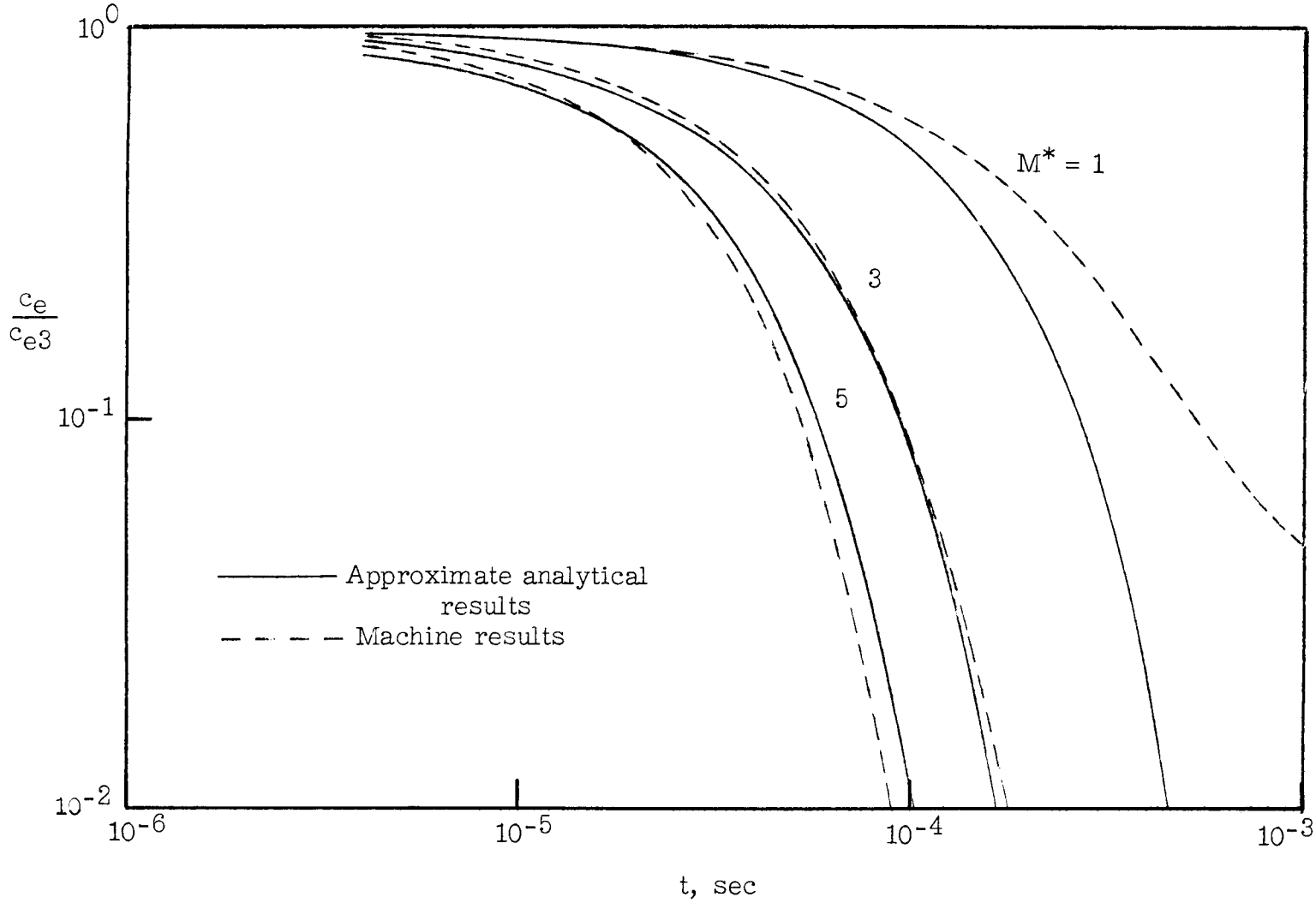

(b) $\frac{c_e}{c_{e3}}$ plotted against t.

Figure 11.- Concluded.

UNCLASSIFIED

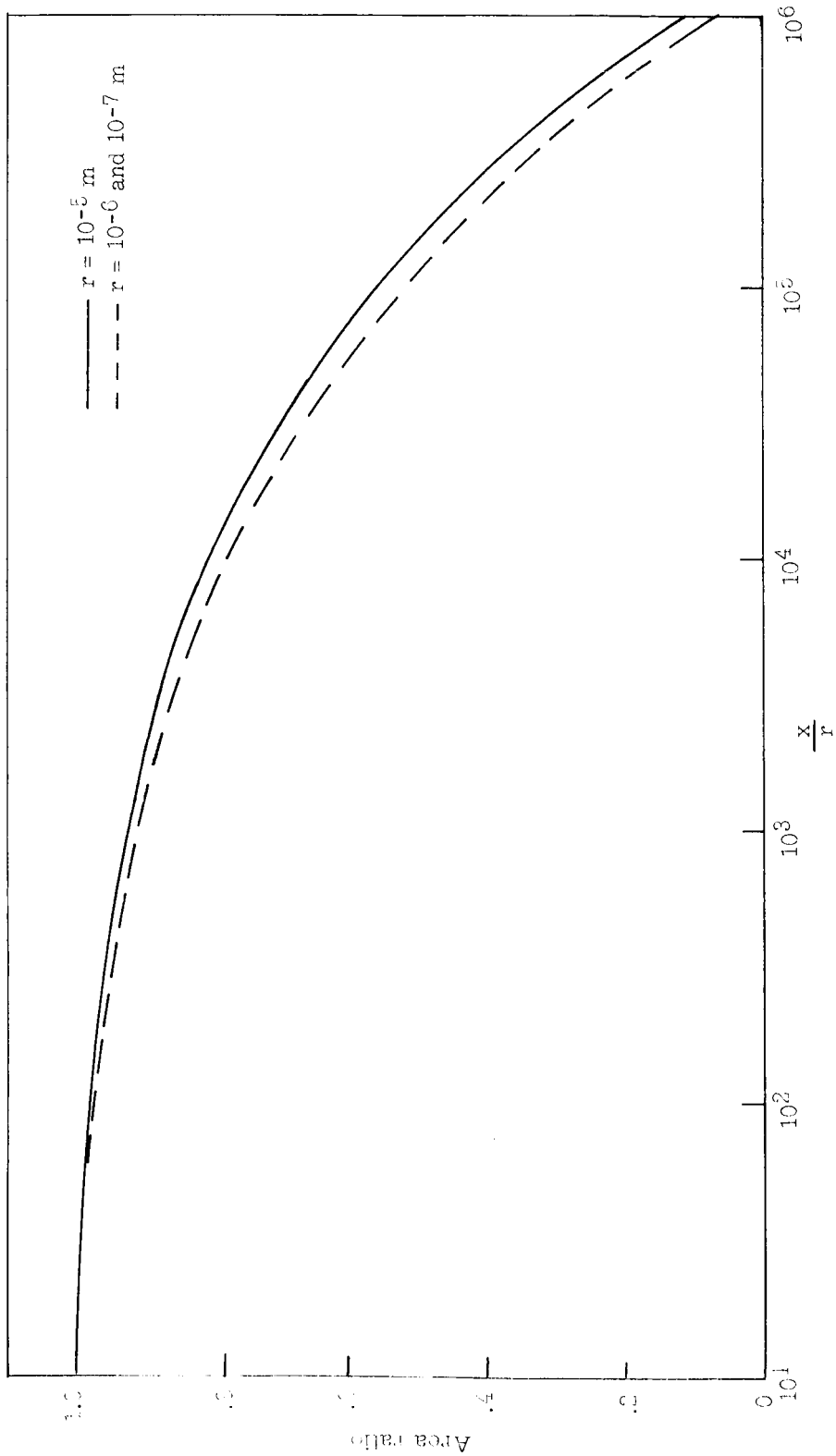

Figure 12.- Ratio of drop surface area to its initial value. Altitude, 4.78×10^4 m (157,000 ft); $M^* = 1.0$. (Computed by using machine program from ref. 21.)